Oxford Research Encyclopedia of Climate Science

Climatic Changes and Cultural Responses During the African Humid Period Recorded in Multi-Proxy Data

David McGee and Peter B. deMenocal

Subject: Regional and Local Climates Online Publication Date: Nov 2017
DOI: 10.1093/acrefore/9780190228620.013.529

Summary and Keywords

The expansion and intensification of summer monsoon precipitation in North and East Africa during the African Humid Period (AHP; c. 15,000–5,000 years before present) is recorded by a wide range of natural archives, including lake and marine sediments, animal and plant remains, and human archaeological remnants. Collectively this diverse proxy evidence provides a detailed portrait of environmental changes during the AHP, illuminating the mechanisms, temporal and spatial evolution, and cultural impacts of this remarkable period of monsoon expansion across the vast expanse of North and East Africa.

The AHP corresponds to a period of high local summer insolation due to orbital precession that peaked at ~11–10 ka, and it is the most recent of many such precessionally paced pluvial periods over the last several million years. Low-latitude sites in the North African tropics and Sahel record an intensification of summer monsoon precipitation at ~15 ka, associated with both rising summer insolation and an abrupt warming of the high northern latitudes at this time. Following a weakening of monsoon strength during the Younger Dryas cold period (12.9–11.7 ka), proxy data point to peak intensification of the West African monsoon between 10–8 ka. These data document lake and wetland expansions throughout almost all of North Africa, expansion of grasslands, shrubs and even some tropical trees throughout much of the Sahara, increases in Nile and Niger River runoff, and proliferation of human settlements across the modern Sahara. The AHP was also marked by a pronounced reduction in windblown mineral dust emissions from the Sahara.

Proxy data suggest a time-transgressive end of the AHP, as sites in the northern and eastern Sahara become arid after 8–7 ka, while sites closer to the equator became arid later, between 5–3 ka. Locally abrupt drops in precipitation or monsoon strength appear to have been superimposed on this gradual, insolation-paced decline, with several sites to the north and east of the modern arid/semi-arid boundary showing evidence of century-scale shifts to drier conditions around 5 ka. This abrupt drying appears synchronous with rapid depopulation of the North African interior and an increase in settlement along the Nile River, suggesting a relationship between the end of the AHP and the establishment of proto-pharaonic culture.

Proxy data from the AHP provide an important testing ground for model simulations of mid-Holocene climate. Comparisons with proxy-based precipitation estimates have long indicated that mid-Holocene simulations by general circulation models substantially underestimate the documented expansion of the West African monsoon during the AHP. Proxy data point to potential feedbacks that may have played key roles in amplifying monsoon expansion during the AHP, including changes in vegetation cover, lake surface area, and mineral dust loading.

This article also highlights key areas for future research. Among these are the role of land surface and mineral aerosol changes in amplifying West African monsoon variability; the nature and drivers of monsoon variability during the AHP; the response of human populations to the end of the AHP; and understanding locally abrupt drying at the end of the AHP.

Keywords: African Humid Period, North Africa, precipitation, monsoon, Holocene, orbital precession, paleoclimate

Introduction

The African Humid Period (AHP) refers to a time from approximately 15,000 to 5,000 years ago during which North and East Africa received substantially more precipitation than at present. During this time, gradual changes in Earth’s orbital precession increased local summer insolation, driving an intensification and northward shift of summer West African monsoonal precipitation (Kutzbach, 1981). In response, the currently hyperarid Sahara Desert (Figure 1) was nearly completely vegetated with grasslands, shrubs, and some tropical woodland vegetation (Hély, Lézine, & Contributors, 2014; Lézine & Casanova, 1989) and contained large and small permanent lakes (Faure, Manguin, & Nydal, 1963; Lézine, Hély, Grenier, Braconnot, & Krinner, 2011; Street-Perrott & Harrison, 1985).

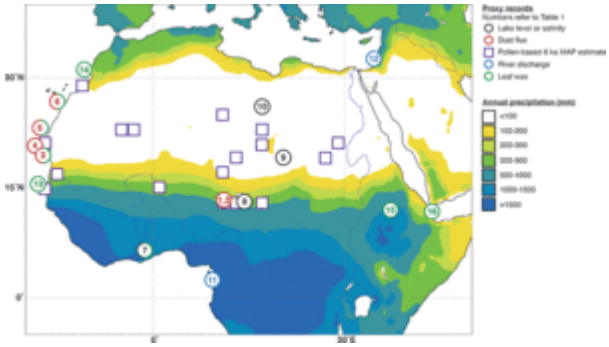

Click to view larger

Figure 1. **Map of Modern Mean Annual Precipitation, Major Rivers and Lakes, and Proxy Sites Discussed in the Text.** Precipitation data are from the NEA CRU TS3p21 dataset of mean precipitation from 1901–2012 (Harris et al., 2014). Numbers on sites refer to site descriptions and references in Table 1 and proxy records plotted in subsequent figures. Colors on site markers indicate proxy type as specified in the legend. Site markers with two colors (sites 3, 5–7) indicate sites with multiple proxy types.

Large river networks developed connecting central Sahara watersheds to the Atlantic and Mediterranean margins (Drake, Blench, Armitage, Bristow, & White, 2011; Skonieczny et al., 2015). Windblown mineral dust emissions from the Sahara dropped by a factor of two to five times relative to current values (McGee, deMenocal, Winckler, Stuut, & Bradtmiller, 2013; Williams et al., 2016). In response, hunter-gatherer and later pastoralist human populations proliferated throughout the modern Sahara and East Africa (Kuper & Kröpelin, 2006; Manning & Timpson, 2014).

The AHP represents the most comprehensive and areally extensive change in low-latitude climate of the last 100,000 years, and it provides an instructive example of the response of continental climate and ecosystems to external forcings (Bony et al., 2015; Hély et al., 2014). Our understanding of changes in African climate and vegetation during the AHP is informed by diverse proxy data from a wide range of terrestrial and marine archives. This wealth of data offers an exceptional opportunity to build a more comprehensive understanding of how climate and vegetation changed during the AHP. This article aims to summarize the key elements of proxy records spanning the AHP, examining the insights that these records provide into the magnitude and spatiotemporal evolution of regional climate changes and land surface responses.

The AHP is typically considered as a regional climate response to orbital precessional forcing of African monsoonal circulation and rainfall. Local summer insolation, taken as the mean June–August (JJA) insolation at 20˚N, peaked around 11–10 ka at values ~8% greater than today, and it was at least 4% greater than today throughout the time between 15 and 5 ka (Figure 2A) (Berger & Loutre, 1991).

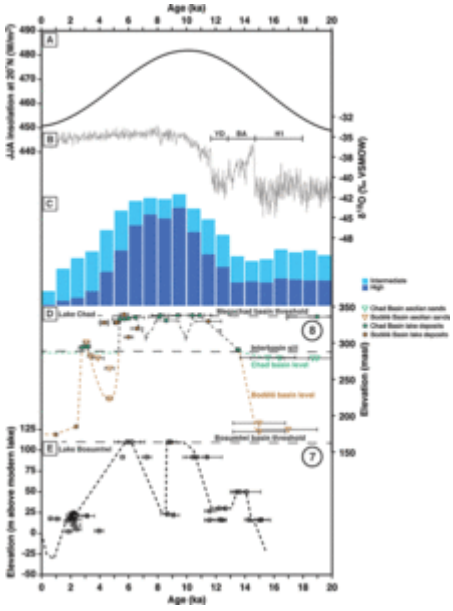

Click to view larger

Figure 2. **Lake Level Records and External Influences on North African Climate Across the African Humid Period.** (A) Mean June–August insolation at 20˚N (Laskar, Fienga, Gastineau, & Manche, 2011). (B) $\delta^{18}O$ values from the North GRIP ice core (Andersen et al., 2004) reflecting high latitude Northern Hemisphere temperatures. H1: Heinrich Stadial 1; BA: Bølling-Allerød warm period; YD: Younger Dryas cold period. (C) Relative abundance of lake basins at low (white), intermediate (light blue). and high water levels (dark blue) for North and East African lakes from the Oxford Lake Level Database (Street-Perrott et al., 1989) and records compiled by Tierney et al. (2011). (D) Lake level reconstruction from Lake Chad near the modern Sahel/Sahara boundary (11–16˚N) (Armitage et al., 2015). Dating control points and schematic lake level curves are shown for the Chad basin (green) and Bodéle basin (gold). Above the interbasin sill elevation, the two basins are integrated into a single lake (black line). (E) Lake level reconstruction from Lake Bosumtwi in tropical West Africa (6˚N). Data compiled by Shanahan et al. (2006); schematic lake level curve redrawn from Shanahan et al. (2015). Circled numbers refer to site locations in Figure 1.

Though low-latitude insolation forcing of summer monsoonal circulation and related feedbacks were the principal drivers leading to enhanced rainfall and deeper monsoonal penetration into the North African subcontinent, this period was also marked by changes in Northern Hemisphere high-latitude climate that substantially impacted North African climate and that are key to understanding proxy records spanning the AHP (Figure 2B) (deMenocal, 2008; Gasse, 2000). Immediately prior to the AHP, Heinrich Stadial 1 (HS1, ~18–15 ka) was marked by pronounced cooling and sea ice expansion in the North Atlantic (Bard, Rostek, Turon, & Gendreau, 2000). Following this period, North Atlantic temperatures warmed dramatically during the Bølling-Allerød period (B-A, 14.6–12.9 ka), then fell again during the Younger Dryas period (YD, 12.9–11.7 ka) (Bard et al., 2000). The beginning of the Holocene was marked by rapid warming of the Northern Hemisphere, but it also included centennial-scale coolings thought to relate to freshwater inputs to the North Atlantic; the largest of these coolings occurred at 8.2 ka (Alley et al., 1997). Throughout the period from 15–7 ka, the Northern Hemisphere ice sheets were retreating (Dyke, 2004), altering mid-latitude atmospheric circulation (Ullman, LeGrande, Carlson, Anslow, & Licciardi, 2014). The proxy

records summarized here document the dual sensitivity of North African climate to low- and high-latitude forcings during the AHP (deMenocal, 2008).

This article examines the major proxy types available for the AHP, including lake level records, vegetation changes, river runoff reconstructions, dust deposition, and the hydrogen isotope composition of leaf waxes. LAKE LEVELS, MINERAL DUST AND DUNE ACTIVITY, VEGETATION DISTRIBUTIONS, RIVER DISCHARGE, and LEAF WAX HYDROGEN ISOTOPE RECORDS summarize proxy records separated by proxy type, examining the interpretation and uncertainties of each proxy. ARCHAEOLOGY relates the proxy data to records of human settlement in the Sahara Desert. PROXY RECORDS OF POTENTIAL FEEDBACKS then examine proxy records that relate to land surface and dust aerosol feedbacks thought to amplify monsoon intensification during the AHP, and GRADUAL OR ABRUPT END OF THE AHP? probes the question of whether the end of the AHP included an abrupt mid-Holocene drop in monsoon strength superimposed on a gradual insolation-paced decline. Locations of key records are summarized in Table 1 and shown in Figure 1. For the sake of brevity and clarity, the article focuses on records from North Africa. For an introduction to East African records of the AHP, we refer to the reader to recent publications (Costa, Russell, Konecky, & Lamb, 2014; Garcin, Melnick, Strecker, Olago, & Tiercelin, 2012; Tierney & deMenocal, 2013; Tierney, Lewis, Cook, LeGrande, & Schmidt, 2011).

Table 1. **Key Proxy Sites Referred to in the Text.** Site numbers refer to site markers in Figure 1

Proxy Type	Site Number (Fig. 1)	Site Name/ Description	Latitude (˚N)	Longitude (˚E)	Reference
Lakes	7	Lake Bosumtwi	6.5	−1.4	Shanahan et al. (2006)
	8	Lake Chad	13.0	14.0	Armitage et al. (2015)
	9	Lake Yoa	19.0	20.3	Kröpelin et al. (2008)
	10	Fazzan Basin	27.0	14.5	Armitage et al. (2007)
Dust	1	Jikariya Lake	13.3	11.1	Cockerton et al. (2014)
	2	Kajemarum Oasis	13.3	11.0	Cockerton et al. (2014)
	3	OC437-7 GC68	19.4	−17.3	McGee et al. (2013)

	4	ODP658C	20.8	−18.6	Adkins et al. (2006)
	5	OC437-7 GC49	23.2	−17.9	McGee et al. (2013)
	6	OC437-7 GC37	26.8	−15.1	McGee et al. (2013)
		OCE205-2 103GGC	26.1	−78.1	Williams et al. (2016)
		VM20-234	5.3	−33.0	Williams et al., 2016
River Discharge	11	MD03-2707	2.5	9.4	Weldeab et al. (2007A,B)
	12	SL112	32.7	34.7	Weldeab et al. (2014)
Leaf Wax δD	7	Lake Bosumtwi	6.5	−1.4	Shanahan et al. (2015)
	13	GeoB9508-5	15.5	−17.9	Niedermeyer et al. (2010)
	3	OC437-7 GC68	19.4	−17.3	Tierney et al. (2017)
	5	OC437-7 GC49	23.2	−17.9	Tierney et al. (2017)

	6	OC437-7 GC37	26.8	−15.1	Costa et al. (2014)
	14	OC437-7 GC27	30.9	−10.6	Tierney et al. (2017)
	15	Lake Tana	12.0	37.3	Costa et al. (2014)
	16	P178-15P	12.0	44.3	Tierney and deMenocal (2013)

Lake Levels

The proliferation and expansion of lakes across North Africa provides perhaps the most concrete evidence of wetter conditions during the AHP. Preserved paleoshorelines and lake sediments document lake and wetland expansions over a broad region of North Africa from 4˚N to 28˚N during the AHP. Here we focus on a north-south transect of influential lake records that offer insights into the spatial and temporal evolution of the AHP and that reflect the range of considerations involved in interpreting lake records.

Beginning in the south, Lake Bosumtwi (6.50˚N, 1.42˚W) is situated within a meteorite impact crater in Southern Ghana that has no outlet beyond a spillway 110 m above modern lake level. Following low levels during Heinrich Stadial 1, the lake rose rapidly after ~14.5 ka during the Bølling-Allerød warm period, reaching levels several tens of meters deeper than today (Figure 2E) (Shanahan et al., 2006). A drop in lake level to elevations approximately 30 m higher than present lake level has been dated to between 12.9 and 12 ka, roughly corresponding to the Younger Dryas stadial (Shanahan et al., 2006). The lake then reached its hydrologic maximum, overflowing at 110 m above present lake level from ~11.5–8.8 ka (Shanahan et al., 2006). Shanahan et al. (2015) interprets an inferred mid-AHP lake level drop near 8 ka to reflect longer summer dry seasons over the lake as the summer rainbelt migrated farther north (see LEAF WAX HYDROGEN ISOTOPE RECORDS for further discussion). High lake levels followed from 7.6–5.4 ka, and deposition of organic-rich, anoxic sediments indicative of deep lake conditions continued until 3.2 ka (Russell, Talbot, & Haskell, 2003). Hydrologic modeling of variations in Lake Bosumtwi suggests that maximum lake levels during the early Holocene require a 6.4–8.2% increase in precipitation, and that low lake levels during HS1 require a ~20% drop in precipitation (Shanahan et al., 2008). The high sensitivity of lake depth to precipitation results from the lake's low surface area:volume ratio. Despite the small magnitude of estimated precipitation changes, these findings provide important constraints on spatial patterns of AHP precipitation changes.

North and east of Lake Bosumtwi lie the Chad and Bodélé basins, the site of Lake Megachad (~12–17˚N, 13–18˚E), which was almost the size of the Caspian Sea during the early Holocene. Whereas the Bosumtwi basin is steep sided, producing large changes in lake elevation for relatively small changes in precipitation and evaporation, the wide, shallow Chad and Bodélé basins produce large changes in lake surface area—and thus evaporative flux—for even minor changes in lake elevation. In the 1960s prior to significant irrigation impacts on lake level, Lake Chad maintained an elevation of 282–283 m and an area of 20,000–25,000 km^2 (Coe & Foley, 2001). Lakes in the Chad basin spill into the Bodélé basin through the Bahr el Ghazal channel at an elevation of 287 m, and they begin overflowing into the Niger River watershed at an elevation of 325 m (Drake & Bristow, 2006). The rise of Lake Megachad began at approximately 13.7–13.4 ka (Armitage, Bristow, & Drake, 2015). Few data exist to document lake level changes during the YD, but OSL dating of alluvial sedimentation on a floodplain in the basin suggests rising lake level

from 12.9–11.5 ka during the YD (Gumnior & Preusser, 2007). The lake reached the threshold of its basin at 325 m by ~11.5 ka and appears to have overflowed nearly continuously until ~5.0 ka (Armitage et al., 2015). During this period the lake would have had an area of 361,000 ± 13,000 km^2 (Drake & Bristow, 2006), and it would have contributed water to the Niger River. Water balance modeling suggests that the lake basin received at least 650 mm/yr of precipitation during its hydrologic maximum, compared to ~350 mm/yr averaged over the basin today (Fraedrich, 2015; Kutzbach, 1980). Short-lived regressions during the AHP are suggested by dating hiatuses at ~10.4–9.4 ka and 8.1–6.6 ka (Armitage et al., 2015), but the precise timing and magnitude of these lake level drops are not known. At the end of the AHP, water levels dropped >100 m in Bodélé basin and 34 m in the Chad basin in a few centuries between ~5 and 4.7 ka. A short-lived rise to 295 m occurred at ~3 ka, with final desiccation of the Bodélé basin at ~1 ka (Armitage et al., 2015).

Just north of the Chad basin lie the Ounianga lakes of northeastern Chad, which occupy multiple deflation basins between the Tibesti and Ennedi mountains. The best studied of these lakes is Lake Yoa (19.03°N, 20.31°E), a small (4 km^2) lake that owes its modern existence to groundwater inputs from the Nubian Sandstone Aquifer System (Grenier, Paillou, & Maugis, 2009); waters discharging in the lake today reflect aquifer recharge during Quaternary pluvial events such as the AHP (International Atomic Energy Agency, 2007). Because of the importance of regional groundwater flow to the lake's water budget, lake levels cannot be used to quantitatively estimate precipitation amounts. Instead, studies of the lake's history have focused on its remarkable sedimentary record, which preserves annual laminations spanning the last 6.1 ka (Francus et al., 2013; Kröpelin et al., 2008). High-resolution mineralogical, elemental, and sedimentological data suggest gradual drying beginning around 5.6 ka and continuing until as recently as 1 ka (Francus et al., 2013). Fossil chironomid and diatom assemblages in the sediments have been used to infer lake salinity, which should track water residence time in the basin. Low salinities are found prior to 4.3 ka, likely to due to outflow of lake water either at the surface or in the subsurface. Salinities rise rapidly between 4.2 ka and 3.8 ka, indicating a reduction of outflow and subsequent concentration of solutes by evaporation (Eggermont et al., 2008; Kröpelin et al., 2008). Taken together with pollen data from the same sediment core (VEGETATION DISTRIBUTIONS), these data have been interpreted as indicating a gradual drying of northeastern Chad tracking summer insolation (Francus et al., 2013; Kröpelin et al., 2008), in marked contrast to the abrupt ~5 ka drying of Lake Chad immediately to the south. An open question, however, is whether the gradual drying recorded at Lake Yoa is primarily due to buffering of its hydrological balance and local vegetation by high groundwater inputs (Grenier et al., 2009).

To the northwest, the Fazzan basin of southwestern Libya (~26˚N, 17˚E) contains deposits suggesting the former presence of a lake extending to ~75,000 km^2 (Armitage et al., 2007; Cremaschi, 2002; Drake et al., 2008). This paleo-lake is noteworthy for being one of the only large lakes fed exclusively by Saharan (as opposed to coastal Mediterranean or Sahelian) rivers. OSL dating of sandy lacustrine sediments grading into a shell-rich beach

deposit indicates that the lake was present between 9 and 11 ka (Armitage et al., 2007). Much less is known about the lake level history in this basin, however, due to a combination of limited access, aeolian deflation, and cover of some shoreline deposits by sand seas active in the late Holocene. As such, the lake's detailed hydrographic history, and its areal extent during the 6 ka timeslice commonly targeted by modeling experiments, are unknown.

This selective review highlights a few common themes and key issues related to paleolake records. Lake basin hypsometry plays a central role in determining the change in lake depth for a given precipitation change. Many basins did not remain hydrologically closed throughout their history due to surface overflow or groundwater inputs/outputs. Groundwater inputs from outside the basin may cause some lakes to exhibit lagged and smoothed responses to precipitation variability. Eolian deflation and cover by sand dunes produces discontinuous records in many lake basins, limiting our ability to produce well-resolved lake level records from many basins.

Despite these limitations and complexities, lake level data clearly document wetter conditions than present over a broad region of North Africa from 4˚N to 28˚N during the AHP (Lézine et al., 2011; Street-Perrott et al., 1989). While some lake expansions can be explained by runoff from regions to the south receiving higher precipitation, the existence of a prominent catchment divide at ~24˚N extending east-west across the central Sahara requires substantial precipitation increases north of this boundary (Drake et al., 2011). Peak lake extents are achieved between 10–7 ka (Figure 2), followed by widespread drying at latitudes from ~17–23˚N between 6–5 ka (Lézine et al., 2011). Wetlands appear to expand somewhat later, achieving maximum areas from 8–6 ka, perhaps reflecting the long response time of aquifer recharge; consistent with a strong role of groundwater supply, wetlands also show a delayed and prolonged drying from ~6–2 ka proceeding from north to south (Lézine et al., 2011). This north-south trend is also found in broader compilations of North African paleohydrological records (see PROXY RECORDS OF POTENTIAL FEEDBACKS) (deMenocal, 2015; Shanahan et al., 2015).

High-resolution (sub-millennial) records reflecting lake water balance do not robustly indicate coherent monsoon variability within the AHP, though this may reflect incomplete records and chronological uncertainties. A number of records suggest rapid drying at ~5 ka; in addition to the Lake Chad record reviewed here, lake level reconstructions from Lakes Turkana (Garcin et al., 2012), Abhe (Gasse & van Campo, 1994), and Ziway-Shalla (Gillespie et al., 1983) in East Africa indicate rapid drying around 5 ka. At present, there is insufficient data to document the spatial extent of this drying event, pointing to the need for more high-resolution lake level reconstructions.

Mineral Dust and Dune Activity

The Sahara is the largest source of mineral dust to the atmosphere, and reconstructions of dust deposition in regional sediments form an essential part of our understanding of North African climate evolution over the last 3 million years (deMenocal, 1995; Larrasoaña, Roberts, Rohling, Winklhofer, & Wehausen, 2003; Trauth, Larrasoaña, & Mudelsee, 2009). Records of dust deposition rates in marine and lacustrine sediments from around North Africa consistently show reduced dust deposition during the AHP. The best known of these records documents terrigenous depositional fluxes at Ocean Drilling Program (ODP) Site 658 off the Mauritanian coast (20.8˚N, 18.6˚W) (Figure 3B) (Adkins, deMenocal, & Eshel, 2006; deMenocal et al., 2000).

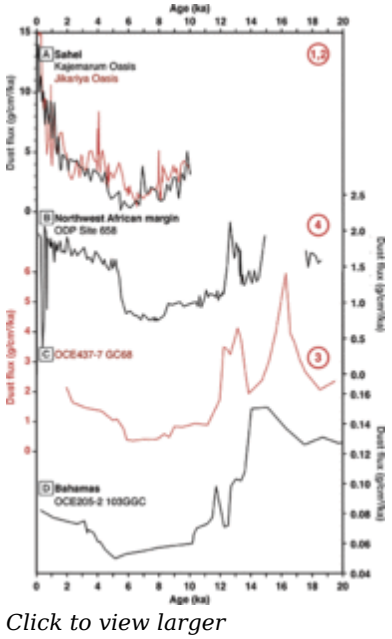

Click to view larger

Figure 3. **Records of North African Dust Deposition Spanning the African Humid Period.** (A) Dust fluxes in two oasis lakes in the Manga Grasslands of Nigeria (Cockerton et al., 2014). (B, C) Dust fluxes along the northwest African margin at (B) ODP Site 658 (21˚N) (Adkins et al., 2006) and (C) in core OCE437-7 GC68 (19˚N) (McGee et al., 2013). (D) Dust fluxes in core OCE205-2 103GGC near the Bahamas (Williams et al., 2016). Circled numbers refer to site locations in Figure 1.

Terrigenous fluxes at this site are interpreted as primarily representing dust deposition. This record shows relatively low dust fluxes from 14.5 ka to ~13 ka, approximately correlative with the Bølling-Allerød warm period. Dust fluxes rise by a factor of almost two during the Younger Dryas cold period. Dust fluxes then fall again after the end of the YD at ~12 ka, and fall progressively from 12–6 ka. Dust fluxes then rise abruptly at ~5.5 ka, doubling over a period of only a few centuries (Adkins et al., 2006; deMenocal et al., 2000).

Subsequent work reproduced the major features of the ODP Site 658 record at three core sites spanning 19–27˚N (Figure 3C) (McGee et al., 2013). This study used grain-size data to estimate the aeolian fraction of terrigenous sediments and thus calculate an aeolian flux rather than a bulk terrigenous flux. As a result of this methodological difference, McGee et al. (2013) suggested larger changes in aeolian dust deposition during the AHP than indicated by the ODP Site 658 record: dust fluxes in the three primary cores in this study were a factor of five lower at 8–6 ka than during 2–0 ka, as opposed to a factor of two at ODP Site 658. A core at 31˚N in this study does not show significantly reduced AHP dust fluxes, either because of its location near a major submarine canyon or because the AHP was expressed differently near this site. These cores have lower sedimentation rates than ODP Site 658

and thus are more strongly smoothed by bioturbation. Use of a simple bioturbation model suggests that the dust flux records measured at the three core sites between 19–27˚N are consistent with an abrupt rise in dust deposition at the end of the AHP. Taken together, the records suggest that this rise occurs at a weighted mean age of 4.9 ± 0.2 ka, slightly later than the age of the rise estimated solely from ODP Site 658 (McGee et al., 2013).

Reconstructions of dust concentration in regional sediments indicate that the reduction in dust deposition during the AHP also extends to sites as far south as 12˚N (Collins, Govin et al., 2013). Recent work has also reconstructed dust deposition over the last 10 ka using lake sediments from two oases in Northeastern Nigeria just west of the Chad basin (Figure 3A) (Cockerton, Holmes, Street-Perrott, & Ficken, 2014). These records indicate minimum dust fluxes at ~8–6 ka, similar to records from the African margin. In contrast to the marine records, these oasis sites indicate a very gradual rise in dust flux beginning after 6 ka, followed by a rapid rise during the last ~1 kyr. This late rise appears to reflect the final desiccation of the Chad and Bodélé basins at ~1 ka along with human influences over the last few centuries (Armitage et al., 2015; Cockerton et al., 2014).

At all of these sites, aeolian inputs are coarse-grained (10–60 µm) and are likely to represent inputs from relatively proximal sources (Cockerton et al., 2014; McGee et al., 2013; Tjallingii et al., 2008). Geochemical and grain-size studies and studies of modern dust storms suggest that the primary sources of dust deposited along the Northwest African margin are likely to be dune fields along the western Saharan coast and sources in Southwestern Algeria and Mali (Lancaster et al., 2002; Skonieczny et al., 2011, 2013), with some authors suggesting that ephemeral lake basins became important sources in the AHP (Cole, Goldstein, deMenocal, Hemming, & Grousset, 2009).

Because the Northwest African and Nigerian records are likely to reflect short-range dust transport from proximal sources, it is uncertain whether they represent changes in the broader Saharan dust plume. New records from the central tropical North Atlantic (VM20-234) and the Bahamas (OCE205-2 100GGC and 103GGC) indicate a very similar dust flux history to West African margin cores (Figure 3D) (Williams et al., 2016). These records suggest that dust deposition at these distal sites was at least 40% lower during the AHP than during the last 2 kyr. As these two sites receive African dust in opposite seasons today (winter in the tropical North Atlantic and summer in the Bahamas), their similarity suggests coherent changes in the winter and summer dust plumes during the AHP. Core VM20-234 has a low sedimentation rate and is not able to constrain the abruptness of the end-AHP rise in dust flux. The Bahamas cores indicate a more gradual rise in dust flux at the end of the AHP than is indicated by cores along the West African margin, with most of the mid-Holocene rise in dust deposition occurring between 5–3 ka (Williams et al., 2016). This difference may reflect the larger number of North African source regions integrated by dust transported to the Bahamas, or the multicentennial to millennial timescales of sediment transport from the Bahama Banks to the core sites (Slowey & Henderson, 2011).

Saharan dust is also transported north into the Mediterranean Sea and eastward into the Arabian Sea. In the Mediterranean, identification of Saharan dust is difficult due to inputs of terrigenous sediments from rivers, local shelves and islands (e.g., Box et al., 2011). Magnetic, geochemical, and mineralogical measurements all suggest a reduction in dust abundance during the AHP (Box et al., 2011; Ehrmann, Seidel, & Schmiedl, 2013; Larrasoaña et al., 2003), but no quantitative dust flux records exist. Farther north, Ti concentrations and Nd isotope data from a peat bog in Switzerland suggest low Saharan dust inputs from 12–7 ka, an increase in Saharan dust inputs relative to local inputs between 7 and 5 ka, and high, stable Saharan inputs after 5 ka (Le Roux et al., 2012). In the Arabian Sea, records suggest a gradual decrease in weathering intensity in the Horn of Africa after 6 ka (Jung, Davies, Ganssen, & Kroon, 2004) and a decrease in dust flux during the early Holocene (Pourmand, Marcantonio, & Schulz, 2004). It is not known whether this Arabian Sea dust flux record primarily reflects North African, Arabian, or South Asian dust sources.

Dune activation ages show similarity to dust deposition records, with multiple regions indicating reduced dune migration during the AHP. Dunes in Western Mauritania—just onshore from ODP Site 658—show periods of activation at 24–15 ka, 13–10 ka (potentially correlative with the Younger Dryas) and after 5 ka, very similar to the timing of high dust fluxes in marine records from the region (Lancaster et al., 2002; Sarnthein, 1978). In the Chad basin, dune migration ends at 15 ± 1.8 ka, and the earliest evidence for reactivation comes at 4.7 ± 0.2 ka (Armitage et al., 2015). Interestingly, there is no evidence for reactivation of dunes during the Younger Dryas in the Chad basin.

The most common interpretation of these records is that increased soil moisture, vegetation density and lake extents during the AHP reduced dust emissions from the land surface and stabilized dunes (Egerer, Claussen, Reick, & Stanelle, 2016, 2017).These land surface changes undoubtedly had an impact, but reduced surface wind speeds may also have played a role in reducing dune activity and dust emissions. Dune activity is a much stronger function of wind speed than of precipitation or vegetation cover (Tsoar, 2005). Further, records of primary productivity and sea surface temperature from the Northwest African margin suggest much-reduced coastal upwelling during the AHP, consistent with reduced northeasterly winds (Adkins et al., 2006; Bradtmiller et al., 2016; Zhao, Beveridge, Shackleton, Sarnthein, & Eglinton, 1995). An aeolian dust and grain-size record produced for a sediment core near Site 658 documents that the AHP and earlier humid phases were associated not only with lower dust concentrations but also much finer grain sizes (Tjallingii et al., 2008), which the authors ascribe to the influence of weaker transporting winds during humid phases, especially compared to the much coarser aeolian grain sizes of cooler stadial events such as the YD and Heinrich events. Recent model simulations seeking to match observed dust flux changes highlight land surface changes as the primary reason for reduced dust emissions in the AHP (Albani et al., 2015; Egerer et al., 2016, 2017). Simulations with prognostic dust emissions, transport, and deposition such as these have the potential to offer improved comparisons between data and models and to test the drivers of observed dust changes, and the results to date point to land surface

changes as the dominant reason for low AHP dust emissions. It is unclear, however, whether these models adequately represent the high-speed wind events responsible for dust emissions and dune activation, or whether the modeled wind changes are sufficient to explain the changes in coastal upwelling accompanying the AHP.

Together, dust flux records suggest highly coherent changes in North African dust plume during the AHP. Dust fluxes along the Northwest African margin at 6 ka were approximately a factor of five lower than during the late Holocene, reflecting reduced emissions from relatively proximal sources, and long-range transport of North African dust across the subtropical North Atlantic was reduced by approximately a factor of two. Dust records consistently point to minimum emissions from 8–6 ka, later than the hydrological maximum of the AHP from ~10–8 ka indicated by lake and river runoff records. This difference could be due to the sensitivity of winds to high-latitude warming and final ice sheet retreat after ~8 ka, or it could reflect the expansion of wetlands in North Africa from 8–6 ka (LAKE LEVELS). Dust records support an abrupt increase in dust emissions from Northwest Africa around 5 ka, but the relative importance of winds and aridity in this transition is not known.

Vegetation Distributions

The AHP was marked by profound changes in vegetation distributions across North Africa. At present, North Africa supports a range of ecosystems from rainforest to hyperarid desert due to its strong north-south precipitation gradient (Figure 1). Fossil pollen assemblages within lake and marine sediments provide the primary means of reconstructing past vegetation distributions on the continent, and analysis of modern data suggests that pollen assemblages accurately record local vegetation (Lézine, Watrin, Vincens, & Hély, 2009).

The review of Jolly et al. (1998) found that at 6 ka, sites throughout the modern Sahara show evidence for grasses and shrubs typical of subtropical steppe and savanna environments, with only two sites in Southern Egypt remaining dominated by desert-associated pollen. Higher elevation sites in northern Chad contain pollen characteristic of temperate xerophytic trees and shrubs and even warm mixed forests at 6 ka (Jolly et al., 1998). Summarizing these data, Hoelzmann et al. (1998) estimated that savanna vegetation extended to approximately 20˚N across most of North Africa at 6 ka, and that steppe vegetation extended to 30˚N. This and other summaries present AHP vegetation changes primarily as northward displacements of existing vegetation zones (Hoelzmann et al., 1998; Ritchie & Haynes, 1987).

Studies focused on individual species rather than on vegetation zones come to a somewhat different conclusion, pointing out that species that currently inhabit distinct Saharan, Sahelian, and tropical Sudanian communities coexisted in the modern Sahara during much of the AHP (Hély et al., 2014; Watrin et al., 2009). These authors also note that the northward progression of individual tropical and Sahelian plant species at the beginning of the AHP occurred at different rates, depending on species' water requirements and ability to spread into new habitat. While pioneer species (e.g., *Alchornea*, *Salvadora*) achieved their northernmost positions as early as 11.8–11.0 ka, other species did not expand northward until more than 1000 years later (Watrin et al., 2009). The slow emplacement of Sahelian and tropical vegetation assemblages in the Sahara at the beginning of the Holocene may thus have as much to do with the speed of species' migration as it does with climatic factors such as the presence of remnant ice sheets.

The most extensive vegetative cover across the Sahara occurred between ~10–8 ka, in substantial agreement with lake level records (Watrin et al., 2009). This time period is also the time of maximum coexistence of Saharan, Sahelian, and tropical taxa, with maximum overlap between 14–19˚N. Tropical-associated species extended as far north as 20–25˚N, 2–7˚ north of their present northernmost occurrence. The diverse coexistence patterns likely reflect colonization of lake margins and river basins by tropical species, while more xeric species inhabited drier portions of the landscape (Watrin et al., 2009).

Compilations of pollen data generally indicate a time-transgressive end to the AHP, with Sahelian and tropical taxa disappearing first from sites in the northern Sahara beginning after ~7–6 ka, but with substantial differences by taxon (Hély et al., 2014; Watrin et al., 2009). The highest-resolution pollen record spanning the end of the AHP comes from Lake Yoa in northeastern Chad (see also LAKE LEVELS). Here, the pollen assemblage at 6 ka includes abundant Poaceae mixed with tropical humid (Sudanian) arboreal taxa, interpreted as reflecting inputs from both extensive regional grasslands and local wadi vegetation. The transition to more xeric species occurs gradually after 4.7 ka, with desert flora becoming fully established only after 2.7 ka (Kröpelin et al., 2008). Taken together, this pollen record is interpreted as reflecting gradual ecosystem change in the surrounding area spanning multiple millennia at the end of the AHP.

Vegetation distributions can also be reconstructed from pollen and fossil leaf waxes deposited in marine sediments. Pollen at ODP Site 658 on the Northwest African margin (20.8˚N, 18.6˚W) shows a sharp increase in Poaceae and Cyperaceae abundance, and a decline in desert-associated pollen such as *Ephedra* and Chenopodiaceae, after 10 ka that persists through the AHP (Dupont, 2011; Dupont, Beug, Stalling, & Tiedemann, 1989; Zhao, Dupont, Eglinton, & Teece, 2003). A similar pattern is observed in sediments at 27˚N (Dupont, 2011). A challenge particular to the Northwest African margin is that strong northeasterly trade winds during the LGM and cool stadial events transported Mediterranean-affinity pollen taxa along the coastline (Dupont, Beug, Stalling, & Tiedemann, 1989), confounding some interpretations.

The carbon isotope compositions of leaf wax compounds (*n*-alkanes) found in marine and lake sediments have been studied as an indicator of the relative contributions of C_3 vs. C_4 plant cover, as C_4 contributions in North Africa are dominated by heat- and aridity-adapted savanna grass vegetation. Plant wax $\delta^{13}C$ values from Lake Bosumtwi sediments (6.5˚N, 1.4˚W) document a very abrupt (century-scale) shift from dominantly C_4 to C_3 vegetation after 14.7 ka, coincident with the onset of more humid conditions deduced from plant wax δD data and lake level increases (Shanahan et al., 2016). This study also noted that the glacial C_4-dominated vegetation was associated with abundant charcoal particles, indicative of extensive landscape burning prior to 14.7 ka. The transition into the AHP after 14.7 ka was marked by a sharp reduction in burning and an abrupt increase in C_3 plant abundance. Additional stepwise increases occurred over the early Holocene, establishing a dominantly C_3 vegetation, low-fire regime that persisted until the last ca. 3 ka BP when drier conditions with more common fires were reestablished.

Surprisingly, leaf wax $\delta^{13}C$ data from marine sediments from Northwest Africa indicate little difference in the C_3/C_4 balance between the AHP and the late Holocene (Castañeda et al., 2009; Collins et al., 2011; Zhao et al., 2003), and some sites even indicate an increase in C_4 abundance during the AHP (Kuechler, Schefuß, Beckmann, Dupont, & Wefer, 2013). The pollen data from ODP Site 658 and terrestrial sites suggest that the reason for this lack of sensitivity is that the wetter early Holocene is associated with a large expansion in the

range of C_4 grasses in North Africa, overwhelming the signature of an increase in C_3 plants in the Sahel (Dupont, 2011; Kuechler et al., 2013).

Pollen data provide the primary means of quantitatively estimating precipitation changes associated with the AHP, allowing quantitative model-data comparisons (Braconnot et al., 2007; Joussaume et al., 1999; Perez-Sanz, Li, González-Sampériz, & Harrison, 2014). The gridded compilation of Bartlein et al. (2011) identifies a total of eleven 2˚ x 2˚ cells between 15–25˚N in North Africa with precipitation estimates for the 6 ka timeslice (Figures 1, 7). While modern precipitation in this latitude range is <100 mm, pollen MAP estimates for 6 ka range from 175–600 mm and generally agree with precipitation anomalies estimated from lake water balance modeling (Figure 7). Interestingly, the pollen-based MAP estimates show no clear change between 17–23˚N, in seeming conflict with early reconstructions indicating a transition from savanna to steppe vegetation across 19˚N (Hoelzmann et al., 1998). The overall increase in ecosystem diversity in the Sahara during the AHP presents a challenge for pollen-based MAP estimates, as many AHP assemblages have no modern analogues (Hély et al., 2014; Hoelzmann et al., 2004; Watrin et al., 2009).

River Discharge

Proxy records of river discharge from North and East Africa show marked increases in river outflow and activation of relict river networks during the AHP. The earliest inferences of past river discharge changes came from studies of sapropel layers (sediments rich in organic matter) in Mediterranean sediments (Rossignol-Strick, 1983; see Rohling, Marino, & Grant, 2015 for a recent review). Deposition of the most recent sapropel is estimated to begin at ~10.5 ka and extend to ~6 ka (Figure 4) (De Lange et al., 2008; Mercone et al., 2000).

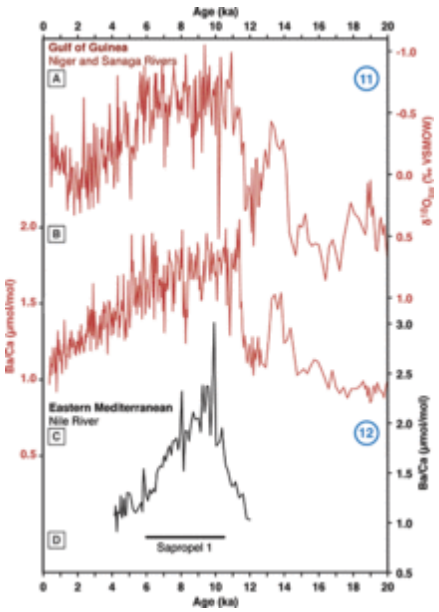

Click to view larger

Figure 4. **Proxy Records of River Discharge from North Africa.** (A) $\delta^{18}O$-seawater values and (B) Ba/Ca reconstructions from planktonic foraminifera in core MD03-2707 in the Gulf of Guinea, taken as proxies for discharge from the Niger and Sanaga Rivers (Weldeab et al., 2007A) Lower $\delta^{18}O$-seawater values and higher Ba/Ca ratios are taken to reflect higher river discharge. $\delta^{18}O$-seawater estimates are corrected for the effect of ice volume on mean seawater $\delta^{18}O$ values. (C) Ba/Ca record from planktonic foraminifera in core SL112 (Weldeab et al., 2014), reflecting Nile River discharge into the Eastern Mediterranean. (D) The estimated duration of the deposition of Sapropel 1 in Eastern Mediterranean sites (De Lange et al., 2008; Mercone et al., 2000). Circled numbers refer to site locations in Figure 1.

Sapropel formation is interpreted to reflect stagnation of deep waters due to stratification of the water column by increased freshwater inputs, chiefly due to increased Nile River discharge (Rohling et al., 2015; Rossignol-Strick, 1983). Oxygen and carbon isotope data from the eastern Mediterranean suggest that an increase in water-column stratification began at ~11.5–11.3 ka, substantially before sapropel deposition (Casford et al., 2002; De Lange et al., 2008). Organic matter accumulation in sediments can also result from increased productivity, but nitrogen isotope values in Mediterranean sediments suggests that the sapropel layers accumulated when the surface ocean was stratified and nutrient-depleted, rather than resulting from elevated surface productivity (Möbius, Lahajnar, & Emeis, 2010; Sachs & Repeta, 1999). In more quickly accumulating sediments, the early Holocene sapropel contains a brief reduction in organic carbon content and Ba/Al ratios (a marker of organic carbon content less prone to diagenetic alteration) at ~8 ka (Mercone et al., 2000).

River runoff can also be reconstructed using Ba/Ca ratios and $\delta^{18}O$ values in planktonic foraminifera. Near river mouths, seawater Ba/Ca ratios rise and $\delta^{18}O$ values fall with increased river discharge due to Ba desorption from riverine sediments in estuaries and low $\delta^{18}O$ values of river water relative to seawater. $\delta^{18}O$ values in planktonic foraminifera are also sensitive to changes in temperature and in the oxygen isotopic composition of river water; use of independent sea surface temperature proxies (Mg/Ca, alkenone undersaturation, planktonic assemblages) can remove the temperature effect and allow estimation of the $\delta^{18}O$ composition of seawater ($\delta^{18}O_{sw}$). In the eastern Mediterranean Sea, a record of Ba/Ca ratios in foraminifera spanning 12–4 ka indicates rising Nile River

discharge from 12–10 ka, maximum discharge from 10–8.5 ka, and gradually decreasing discharge from 8–4 ka (Figure 4C) (Weldeab, Menke, & Schmiedl, 2014). A $\delta^{18}O_{sw}$ reconstruction from the Aegean Sea over the same timespan similarly indicates a steep decline in salinity from 11–10 ka and minimum salinities from ~10–8 ka (Marino et al., 2009). Planktonic $\delta^{18}O$ values and sediment provenance data from a longer record just north of the Nile delta suggest that the increase in Nile discharge began around 14 ka during the Bølling-Allerød warm period, decreased during the Younger Dryas cold period, and then rose again at the end of the Younger Dryas (Revel et al., 2010). The fact that this early rise in Nile discharge did not result in water-column stratification or sapropel deposition may reflect the impact of post-glacial sea level rise on the buoyancy budget of Mediterranean surface waters (Rohling et al., 2015). Overall, Nile discharge records show good agreement with the interpretation of the early Holocene sapropel in eastern Mediterranean sediments (Rohling et al., 2015).

Ba/Ca and $\delta^{18}O_{sw}$ records have also been used to reconstruct the outflow of the Niger-Benue and Sanaga Rivers into the Gulf of Guinea (Weldeab, Lea, Schneider, & Andersen, 2007A). The Niger-Benue watershed drains a large portion of West Africa, and also included inputs from the Chad basin when Lake Megachad was at its threshold during the AHP (Figure 2D). The Sanaga River drains a smaller region in low-latitude central Africa. These records indicate low discharge during the Last Glacial Maximum and Heinrich Stadial 1, followed by a rise beginning at 14.5 ka during the Bølling-Allerød warm period and a fall during the Younger Dryas (Figure 4A, B) (Weldeab et al., 2007A). High discharge occurs during the early Holocene from 11.4 ka to 5.1 ka, with peak Ba/Ca values and minimum $\delta^{18}O_{sw}$ values from ~11.4–8 ka and gradually declining Ba/Ca ratios thereafter. Several century-scale reductions in Ba/Ca ratios occur during the AHP, with the most prominent occurring at ~10.9 ka, 9.2 ka, and 8.2 ka. These times coincide with cooling events in the high-latitude North Atlantic (Weldeab, Lea, Schneider, & Andersen, 2007B). The decline in Ba/Ca and inferred river discharge into the Gulf of Guinea proceeds through the late Holocene, with a small step to lower values at ~5 ka. This drop may reflect the cessation of inputs from the Chad basin after Lake Chad dropped below its overflow threshold into the Niger watershed at this time (Armitage et al., 2015).

Several currently inactive river drainages in the Sahara became active during the AHP. One such drainage is the lower Wadi Howar in the Nubian desert of central Sudan. Here, a variety of geologic and faunal evidence points to this drainage having been active during much of the AHP (Pachur & Kröpelin, 1987). This watercourse extended over 400 km from the current terminus of the upper Wadi Howar to the Nile, connecting the eastern central Sahara to the Nile. Remote sensing data and GIS analysis also indicate the existence of large relict drainages in both the western and northern Sahara. These include the extensive Tamanrasett watershed reaching westward from the north-central Sahara to the Mauritanian coast (Skonieczny et al., 2015) and the Sahabi and Kufrah watersheds extending northward from the central Sahara through eastern Libya (Ghoneim, Benedetti, & El-Baz, 2012; Paillou et al., 2009; Paillou, Tooth, & Lopez, 2012; Robinson, El-Baz, Al-Saud, & Jeon, 2006). Though limited dating exists for each of these

drainages, the presence of well-preserved alluvial fans in satellite imagery and the abundance of human artifacts (Ounanian points) in each of these watersheds suggests that they were active in the early Holocene (Drake, Blench, Armitage, Bristow, & White, 2011).

These relict drainages indicate that the central Sahara was hydrologically connected to coastal or near-coastal regions in the Mediterranean and the western Sahara in the early Holocene. The modern distribution of fish species across the Sahara (e.g., *Tilapia zillii*) also suggests that riparian corridors efficiently crossed the region from north to south in the past, and the presence of hippopotamus and crocodile remains in the center of the modern Sahara indicate that relatively deep waters were present in many sites year round (Drake et al., 2011). Together, these data suggest that water courses provided a nearly complete connection for human migration across the Sahara during the early Holocene and previous humid periods (Drake et al., 2011).

In summary, river reconstructions support higher river discharge and widespread activation of currently dry river networks during the AHP in both North and East Africa. River discharge reconstructions are valuable for producing spatially averaged precipitation records at high temporal resolution. These reconstructions support a precipitation maximum from ~10–8 ka, similar to lake level records. They also indicate centennial-scale reductions in monsoon strength in response to early Holocene high-latitude cooling events. River discharge data do not suggest longer-duration reductions in precipitation during the AHP, in contrast to lake (LAKE LEVELS) and leaf wax hydrogen isotope records (LEAF WAX HYDROGEN ISOTOPE RECORDS), perhaps due to the larger spatial scales averaged by the Nile and Niger-Benue watersheds.

Leaf Wax Hydrogen Isotope Records

Records of the hydrogen isotope composition of leaf wax compounds (δD_{wax}) preserved in lake and marine sediments provide a means of inferring past changes in precipitation δD and terrestrial aridity. Precipitation δD (δD_{precip}) reflects local precipitation amount and water vapor history, with greater rainout from an airmass leading to lower δD_{precip}, and recycling of moisture leading to higher δD_{precip} (Dansgaard, 1964; Risi, Bony, & Vimeux, 2008; Risi, Bony, Vimeux et al., 2008). δD_{wax} responds to changes in δD_{precip} but is also impacted by fractionation within the plant and evaporation of soil and leaf water. As greater evaporation of soil and leaf water, reduced rainout, and a greater relative importance of recycled moisture all increase δD_{wax}, higher δD_{wax} values are generally interpreted qualitatively as reflecting drier conditions (Kuechler et al., 2013; Sachse et al., 2012), but some studies have tried to quantitatively infer δD_{precip} from δD_{wax} values (Collins, Schefuß et al., 2013; Tierney et al., 2017).

δD_{wax} records from marine sediments along the West African coast indicate that mid-Holocene (8–6 ka) δD_{wax} values were 5–20 ‰ lower than late Holocene values at sites between 5˚S and 31˚N after correction for vegetation type (Collins, Schefuß et al., 2013; Tierney, Pausata, & deMenocal, 2017). This decline in δD_{wax} values is consistent with enhanced monsoon strength across a wide region of West Africa during the mid-Holocene as well as a significant northward expansion of monsoon rainfall.

The highest-resolution δD_{wax} record from the region comes from Lake Bosumtwi, Ghana (6.50˚N, 1.42˚W) (Figure 5B).

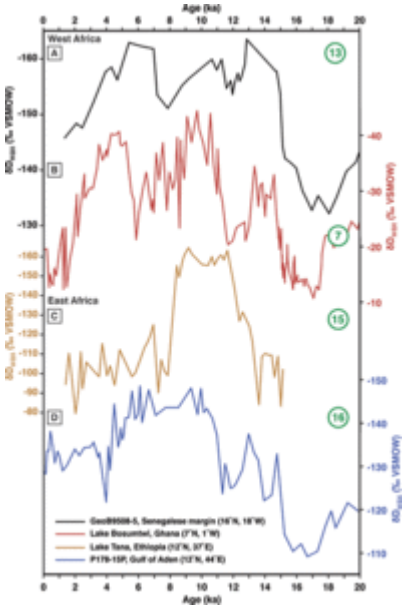

Click to view larger

Figure 5. **Leaf Wax Hydrogen Isotope (δD_{wax}) Records from Sites in West and East Africa.** West Africa: (A) record from marine core GeoB9508-5 from the Senagalese margin (black; Niedermeyer et al., 2010) and (B) lake sediment core record from Lake Bosumtwi, Ghana (red; Shanahan et al., 2015). East Africa: (C) lake sediment core record from Lake Tana, Ethiopia (gold; Costa et al., 2014), and (D) record from marine core P178-15P, Gulf of Aden (blue; Tierney & deMenocal, 2013). All data are corrected for the impact of changing ice volume on mean ocean δD. Circled numbers refer to site locations in Figure 1.

Here, δD_{wax} values fall steeply between 15–14 ka, consistent with a rapid intensification of the West African monsoon across the transition from Heinrich Stadial 1 to the Bølling-Allerød warm period (Shanahan et al., 2015). δD_{wax} values rise during the Younger Dryas cold period (12.9–11.7 ka), then fall to their lowest values from 11.1–9.4 ka, signaling that at low latitudes the West African monsoon was most intense during the early Holocene. δD_{wax} values then gradually rise from 8.5–5.6 ka before moving back to low values between 5.4–3.2 ka. This δD_{wax} record has a good deal in common with the lake level record from Lake Bosumtwi described earlier (Figure 2). Both datasets point to the initiation of wetter conditions during the Bølling-Allerød, drying during the Younger Dryas, high precipitation during the earliest Holocene, and a return to drier conditions after ~8–9 ka. One significant point of difference is that δD_{wax} data indicate that the mid-Holocene dry interval extended to 5.6 ka followed by increased precipitation, while the lake level data suggest high, overflowing conditions from 7.6–5.4 ka, followed by a gradual lowering of lake levels (Shanahan et al., 2008; Shanahan et al., 2015).

δD_{wax} records from a transect of cores spanning 15–31˚N along the Northwest African margin offer improved constraints on the spatial and temporal evolution of monsoon rainfall in Northwest Africa during the AHP (Figure 5A) (Niedermeyer et al., 2010; Tierney et al., 2017). δD_{wax} values fall 15–20 ‰ at ~15 ka in cores at 15˚N and 19˚N but show little change in cores to the north, suggesting that monsoon rainfall during the Bølling-Allerød did not penetrate north of 19˚N in this region. δD_{wax} values throughout the transect rise during the Younger Dryas, then fall to low values at all sites in the early Holocene, suggesting that monsoon rainfall extended to 31˚N in Northwest Africa at this time (Tierney et al., 2017).

A shift back to more positive δD_{wax} values occurs at sites from 15–23˚N at 8–7 ka (Niedermeyer et al., 2010; Tierney et al., 2017), similar to the indications of drying noted above in the Lake Bosumtwi δD_{wax} and lake level records. Shanahan et al. (2015) interpret this mid-AHP drying to indicate that from ~8–6 ka the summer rain belt spent less time at low-latitude sites such as Lake Bosumtwi, leading to a longer summer dry season; in the earliest Holocene and the period after ~6 ka, the less extreme seasonal migration of the rainbelt combined with an intensified monsoon led to an increase in rainfall in the Bostumwi Basin (Shanahan et al., 2015). Tierney et al. (2017), however, show that the drying at ~8 ka is widespread in North and East Africa and suggest that the event is a response to high-latitude cooling associated with freshwater inputs into the North Atlantic during the 8.2 kyr event. These authors suggest that the extended duration of the event (at least 1 kyr, whereas temperature changes during the 8.2 kyr event lasted only a few centuries) results from vegetation feedbacks (Tierney et al., 2017). Further evaluation of this hypothesis will require investigation of why mineral dust and river runoff records from the region do not show the 8–7 ka drying, as well as further development of high-resolution, well-dated vegetation and climate records to better document the timing and magnitude of this event.

Minimum δD_{wax} values persist for the shortest amount of time at the northernmost site on the Northwest African margin (31˚N), consistent with a shorter duration of the AHP in far Northern Africa. Bioturbation modeling of the end of the AHP in δD_{wax} records from 19–27˚N suggests that the records are consistent with an abrupt drying at 5.2±0.3 ka (Tierney et al., 2017), matching the timing of the abrupt rise in dust flux inferred from the same cores (McGee et al., 2013). δD_{wax} values then rise gradually from 5–0 ka throughout Northwest Africa (Niedermeyer et al., 2010; Tierney et al., 2017).

At Lake Tana in Ethiopia (12˚N, 37˚E), δD_{wax} data also suggest an abbreviated AHP maximum, with minimum values occurring only from 11.5–8.5 ka (Figure 5C) (Costa et al., 2014). As these authors point out, runoff and lake level data from the region, including data from Lake Tana, suggest a longer AHP maximum extending from 11.5–5 ka (Gasse & Van Campo, 1994; Gillespie, Street-Perrott, & Switsur, 1983; Marshall et al., 2011). This clear difference between δD_{wax} and independent water balance data suggests that there was a change in water vapor transport paths reaching the lake’s catchment at 8.5 ka, perhaps due to a shift of the Congo Air Boundary, but that precipitation amounts remained high

for a substantially longer period (Costa et al., 2014). Farther east, a site thought to have remained east of the Congo Air Boundary throughout the AHP (and thus to reflect primarily Indian Ocean moisture sources) shows a longer period of depleted δD_{wax} values, with low values from ~10–5 ka (Figure 5D) (Tierney & deMenocal, 2013).

The continuing emergence of δD_{wax} records is shedding new light on the evolution of the AHP, providing reconstructions with high temporal resolution and increasing spatial coverage. These isotopic records support monsoon intensification and expansion during the AHP, and document a millennial-scale excursion during the middle of the AHP toward more positive values at sites in West Africa. Like all proxies, the utility of δD_{wax} records is increased when they can be compared with other hydrological data. δD_{wax} is sensitive to variables such as water vapor source, convective intensity and boundary-layer humidity in addition to local precipitation amount; as a result, differences between co-located δD_{wax} and lake level records, as observed at Lake Tana and Lake Bosumtwi, should be further investigated to provide a more multidimensional view of past monsoon changes and of the interpretation of δD_{wax} data (e.g., Costa et al., 2014; Shanahan et al., 2015).

Archaeology

As he crossed by caravan from Tripoli to Timbuktu in the mid-1800s, German explorer Heinrich Barth became the first European to discover the then-mysterious prehistoric Saharan rock paintings and engravings dating from the AHP. These images depict pastoral scenes with abundant elephants, giraffe, hippos, aurochs, and antelope, occasionally being pursued by bands of hunters. Across North Africa, cave walls and rocky outcrops are adorned with elaborate engravings and paintings of life on this once-pastoral landscape. The incongruence of these lively images in such lifeless settings intrigued Barth, who noted that the art work “bears testimony to a state of life very different from that which we are accustomed to see now in these regions” (Barth, 1857).

The archaeological record of human occupation during the AHP is well documented across the arid expanses of North Africa. Over one thousand sites have been described and, collectively, they present a compelling narrative of quotidian human activity, cultural development, and interactions with a changing external world. This is, arguably, one of the best-documented and expansive examples of human responses to large-scale and rapid climate change.

Manning and Timpson (2014) recalibrated radiocarbon dates for 1011 archaeological sites across North Africa (Figure 6A).

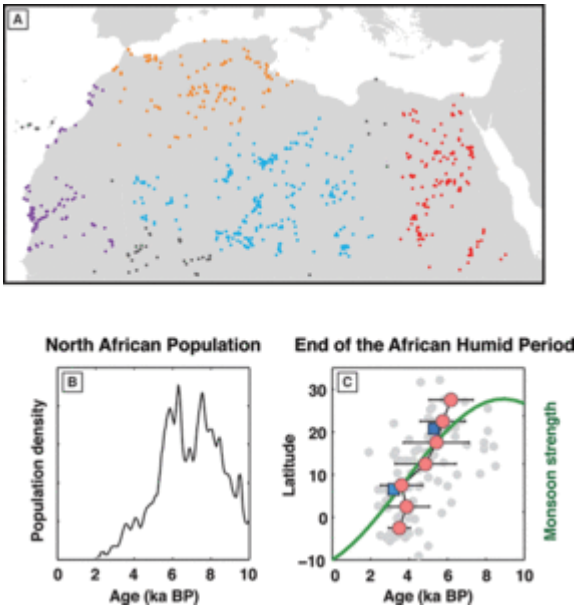

Click to view larger

Figure 6. **Records of Human Habitation of the Sahara During the AHP and a Compilation of Hydrological Proxy Data Spanning the End of the AHP.** (A) Archeological sites dated to the AHP in North Africa (modified from Manning & Timpson, 2014 . Colors denote geographic groupings used in the original paper's analysis. (B) Estimate of North African population derived from Monte Carlo Summed Probability Distribution using all radiocarbon dates from Neolithic sites (Manning & Timpson, 2014; deMenocal, 2015). (C) Estimates of the end of the AHP in proxy datasets compiled from across North Africa (Shanahan et al., 2015) plotted against site latitude (gray circles). Red circles show averages for zonally binned data; blue squares show age estimates for the end of the AHP from Lake Bosumtwi (6.5˚N) and dust flux records from offshore Mauritania (20˚N) (deMenocal, 2015).

Using a Monte-Carlo Summed Probability Distribution (SPD) method that permits combining probability distributions for a large number of dates, they estimated the population density changes in North Africa throughout the Holocene. The approach assumes taphonomic biases, known and unknown, can be overcome with a large number of dates (n = 3287) from a large number of sites (1011) covering a large geographic range.

The SPD population proxy reveals a peak in North African human populations between ca. 9–5 ka BP (Figure 6B). Impressively, the SPD record also reveals a large and rapid depopulation step between 6.3–5.2 ka BP that coincides within a few centuries with the shift toward more arid conditions that defined the end of the AHP. The depopulation was evidently spatially coherent and tracked the retreat of the monsoonal rains. An animation of geographic unfolding of this demographic shift is presented in Manning and Timpson (2014). This reveals that the northernmost sites were abandoned first (near 7–6 ka), whereas they persisted at southernmost sites until the latest Holocene (near 3–2 ka) in agreement with the paleohydrologic proxy data (deMenocal, 2015; Shanahan et al., 2015) and consistent with orbital monsoon theory (Kutzbach & Guetter, 1986).

Where did these people go? One of the more intriguing consequences of this climatic transition and demographic shift was the near synchronous appearance of proto-pharaonic culture along the Nile River. Kuper and Kröpelin (2006) compiled radiocarbon dates from over 150 sites in the eastern Sahara. Their analysis suggested that the large-scale exodus from the Egyptian Sahara coincided with the rise of sedentary life along the Nile. They observe that the first Neolithic communities near Fayum and Merimde appear

near 7 ka BP. Hyperarid desert conditions were established in Egypt by 5.5–5.0 ka BP, after which archaeological records document initial stages of pharaonic civilization along the Nile valley. The first step pyramid at Djoser is dated near 4.6 ka BP, marking the emergence of proto-dynastic culture immediately following this climate-driven settlement of the Nile valley.

Proxy Records of Potential Feedbacks

Simulation of the climate response to 6 ka boundary conditions and forcings—chiefly increased insolation seasonality in the Northern Hemisphere, and reduced seasonality in the Southern Hemisphere—has been a common target of climate model experiments (Braconnot et al., 2007; Joussaume et al., 1999). Both atmosphere-only and coupled ocean-atmosphere general circulation models (GCMs) consistently underestimate the magnitude and northward extension of monsoon precipitation in North Africa estimated from pollen and lake data (Figure 7) (Braconnot et al., 2007; Perez-Sanz et al., 2014).

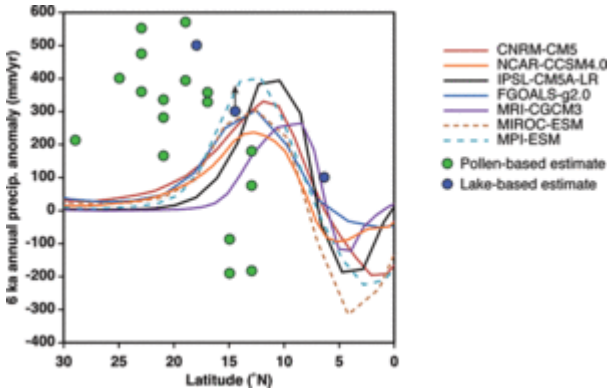

Click to view larger

Figure 7. **Data-Model Comparison for North Africa in the Mid-Holocene.** Green dots show pollen-based estimates of 6 ka precipitation anomalies based on precipitation estimates from Bartlein et al. (2011) and precipitation data from the UEA CRU TS3p21 1901–2012 climatology for the same locations (Harris et al., 2014). Blue dots show precipitation anomalies based on lake shoreline data and water balance modeling for Lake Bosumtwi (6.5˚N) (Shanahan et al., 2008), Lake Chad (12–17˚N) (Kutzbach, 1980), and the West Nubian Paleolake (16–20˚N) (Hoelzmann, Kruse, & Rottinger, 2000); arrow above dot for Lake Chad indicates that this value is a minimum estimate. Lines show modeled precipitation anomalies for mid-Holocene simulations relative to preindustrial simulations averaged over 20˚W–30˚E for a representative set of fully coupled ocean-atmosphere general circulation models included in the Paleoclimate Model Intercomparison Project, version 3 (Braconnot et al., 2012). Dashed lines are

model simulations that included interactive vegetation.

While pollen data are generally interpreted as requiring precipitation anomalies of at 200–300 mm/year from 20–30˚N at 6 ka (Bartlein et al., 2011; Braconnot et al., 2007), models typically simulate peak precipitation anomalies between 10–15˚N and increase precipitation by <100 mm/year at 20–30˚N (Perez-Sanz et al., 2014).

Efforts to understand the cause of the underestimation of West African monsoon enhancement at 6 ka by GCMs have focused on changes in vegetation, lake areas, and windblown dust emissions. Standard 6 ka simulation protocols in the Paleoclimate Modeling Intercomparison Project do not include changes in any of these parameters (Taylor, Stouffer, & Meehl, 2012). The importance of these feedbacks is explored in detail by Claussen et al. (Claussen, Dallmeyer, & Bader, 2017); here we review the constraints that proxies offer on the land surface and dust aerosol changes at 6 ka.

As summarized, pollen data suggest a widespread increase of vegetation in the modern Sahara, with grasses, shrubs, and isolated tropical woodland species occupying the region from 14–25˚N through much of the AHP (Hély et al., 2014; Watrin et al., 2009). This expansion would substantially reduce the land surface albedo and increase moisture recycling, increasing the moist static energy of boundary-layer air north of the modern Sahel-Sahara boundary (Claussen, 2009; Claussen, Brovkin, Ganopolski, Kubatzki, & Petoukhov, 1998; Ganopolski, Kubatzki, Claussen, Brovkin, & Petoukhov, 1998; Patricola & Cook, 2008). A challenge of including these impacts in simulations is that the data document the presence of savanna vegetation and other species in the Sahara at 6 ka, but they do not constrain the density of this vegetation. Comparisons with modern pollen assemblages are made more difficult by the fact that AHP assemblages have no true modern analogues. It is thus difficult to estimate the albedo and leaf-area index that characterized the land surface between 14–30˚N during the AHP; albedos for the Sahara region used in “Green Sahara” simulations range from 0.15 to 0.25 (e.g., Patricola & Cook, 2007; Pausata, Messori, & Zhang, 2016).

Sediments and shoreline features document a widespread expansion of lakes and wetlands between 14–28˚N during the AHP (Hoelzmann et al., 1998; Lézine et al., 2011). GCM experiments incorporating these lakes and wetlands into 6 ka simulations have found that these water sources substantially increase summer precipitation in the northern-central Sahara (Coe & Bonan, 1997; Krinner et al., 2012), though this conclusion is not supported by all studies (Contoux et al., 2013). Hoelzmann et al. (1998) estimated that lakes and wetlands covered ~7.4% of the land surface from 10–30˚N, 17˚W–60˚E (including the Arabian peninsula) during the core of the AHP (~9.5–5.5 ka), with this coverage reaching 14% in the eastern Sahara due to the presence of Lake Chad and comprising only 2% in the western Sahara. The more recent compilation of Lézine et al. (2011) indicates that the peak of lake coverage occurred between 10–7 ka and declined rapidly thereafter, suggesting that the estimates of Hoelzmann et al. (1998) may overstate lake coverage for the 6 ka timeslice. Hoelzmann et al. (1998) point out, however, that the

youngest portion of AHP lake deposits may have been removed by deflation in many basins, causing compilations of lake deposit ages such as Lézine et al.'s (2011) to underestimate lake coverage at 6 ka. Further development of high-resolution lake level records in the central and northern Sahara will be key to improving constraints on lake coverage used in 6 ka model experiments.

Finally, several studies document reduced Saharan dust emissions at 6 ka (Adkins et al., 2006; deMenocal et al., 2000; McGee et al., 2013; Williams et al., 2016). Dust absorbs and scatters incoming solar radiation and also absorbs longwave radiation, impacting top-of-atmosphere and surface radiation budgets and warming the mid-troposphere (Miller, Tegen, & Perlwitz, 2004). Several studies have explored the impact of dust loading over the continent on modern North African precipitation, with no clear consensus on the magnitude or sign of its impacts (Huang, Zhang, & Prospero, 2009; Marcella & Eltahir, 2014; Rosenfeld, Rudich, & Lahav, 2001; Yoshioka et al., 2007). These different results may be due to differences in the radiative properties, grain size, and altitude of dust in these simulations. The impacts of dust loading over the continent are also highly sensitive to surface albedo; today, dust's impacts on longwave and shortwave radiation at the surface nearly cancel due to the Sahara's high albedo, but dust would have had a much more significant negative impact on surface radiation over a lower-albedo Green Sahara during the AHP. As a result, reduced dust loading at 6 ka may have acted to substantially warm the land surface, enhancing the northward extension of monsoon rains (Pausata et al., 2016).

Dust's direct radiative impacts may also be important over the ocean, as the Saharan dust plume is estimated to have a net surface radiative impact of -7.4 ± 1.5 W/m^2 over the tropical North Atlantic (Ridley, Heald, & Prospero, 2014). Dust thus acts to cool the sea surface (Evan, Vimont, Heidinger, Kossin, & Bennartz, 2009), potentially acting to weaken the West African monsoon both through altered surface pressure gradients and decreased specific humidity in air advected onto the continent. A recent simulation found that reducing dust over the tropical North Atlantic by 50%—the approximate reduction in the long-range Saharan dust plume indicated by sedimentary records in the Bahamas and the central North Atlantic—substantially increased precipitation in Northwest Africa (Williams et al., 2016). Again, these findings require further testing to determine their dependence on dust's optical properties and other model-specific parameters (Albani et al., 2014; Pausata et al., 2016; Williams et al., 2016).

With the publication of new records constraining long-range transport of fine-grained Saharan dust (Williams et al., 2016), we may be at a point where uncertainties in the importance of dust as an amplifier of AHP climate come more from model parameters than from a lack of paleo data. Even as progress is made in reducing uncertainties in dust's direct radiative effects (e.g., Albani et al., 2014), modeling of dust's indirect effects on cloud formation is in its infancy (e.g., Gu et al., 2012) and represents an additional potential mechanism by which dust may have modulated orbital forcing of North African climate. Dust is thought to impact cloud formation processes both over the continent and

over the subtropical North Atlantic, with radiative impacts that may equal or surpass its direct radiative effects (Doherty & Evan, 2014; Gu et al., 2012; Kaufman, Koren, Remer, Rosenfeld, & Rudich, 2005). Further work will be required to examine the importance of these indirect effects in response to reduced dust loading in the AHP.

A more basic constraint on dust-related impacts on the AHP is that dust records consistently document that minimum dust fluxes occurred from ~8–6 ka (Adkins et al., 2006; Cockerton et al., 2014; McGee et al., 2013; Williams et al., 2016), while many hydrological and vegetation records suggest that peak monsoon expansion and intensification occurred earlier, from ~10–8 ka (e.g., Costa et al., 2014; Shanahan et al., 2015; Watrin et al., 2009; Weldeab et al., 2007a; Weldeab et al., 2014). Dust may have amplified changes in monsoon strength, particularly at the end of the AHP, but its distinct temporal evolution suggests that its importance was not constant throughout the AHP.

Gradual or Abrupt End of the AHP?

The feedbacks that help explain the magnitude of AHP climate change (PROXY RECORDS OF POTENTIAL FEEDBACKS) also predispose North Africa to abrupt responses to gradual changes in climate forcings. Initial explorations proposed that vegetation/surface albedo feedbacks introduce instabilities in regional climate (Charney, 1975). Later, modeling experiments demonstrated that amplifying feedbacks between vegetation and precipitation create the potential for rapid, nonlinear changes in North African precipitation in response to gradual climate forcing (Claussen et al., 1998; Claussen et al., 1999).

Consistent with these modeling studies, several datasets have suggested an abrupt (century-scale or faster) end of the AHP in response to the gradual decline in summer insolation. The record of terrigenous sediment accumulation at ODP Site 658 documents an abrupt, century-scale doubling of windblown dust fluxes from Northwest Africa at 5.5 ka (Adkins et al., 2006; deMenocal et al., 2000). Dust flux reconstructions from three additional Northwest African margin sites from 19–27˚N are consistent with an abrupt rise in dust deposition at the end of the AHP, with a weighted mean age estimate of 4.9 ± 0.2 ka (McGee et al., 2013). Modeling of North African dust emissions indicates that the observed abrupt rise in dust fluxes requires a similarly abrupt decline in vegetation density and lake area in Northwest Africa; it does not appear that regional dust fluxes can abruptly rise in response to a gradual change in vegetation or lake area (Egerer et al., 2017). Opal fluxes in Northwest African margin sediments rise similarly abruptly at this time, suggesting a rapid invigoration of coastal upwelling at the end of AHP as well (Adkins et al., 2006; Bradtmiller et al., 2016). δD_{wax} records from the same sites also suggest abrupt end-AHP drying at 5.2 ± 0.3 ka (Tierney et al., 2017).

Other records from North and East Africa show evidence for abrupt drying at ~5 ka. These include the high-resolution lake level record from Lake Chad described earlier (Armitage et al., 2015), lake level reconstructions from Lakes Turkana, Abhe, and Ziway-Shalla in East Africa (Garcin et al., 2012; Gasse & Van Campo, 1994; Gillespie et al., 1983), a record of terrigenous sediment accumulation in Lake Tana (Marshall et al., 2011), and δD_{wax} records from several sites in East Africa (Tierney & deMenocal, 2013). Taken together with the dust reconstructions from Northwest Africa, these records suggest that there may have been an important weakening of the West African monsoon system at approximately 5 ka, with maximum impacts at the northern and eastern edges of the summer monsoon's range.

Of course, many proxy records do not suggest an abrupt end to the AHP. These include the high-resolution pollen and lake salinity records from Lake Yoa in northern Chad (Kröpelin et al., 2008), leaf wax records from Lake Bosumtwi (Shanahan et al., 2015) and the Northwest African margin (Niedermeyer et al., 2010), records of river discharge from the Nile and Niger/Sanaga drainages (Weldeab et al., 2007A,B, 2014), and dust flux reconstructions from near the Chad basin (Cockerton et al., 2014). It must be emphasized, however, that several factors conspire against the recording of an abrupt change in proxy records. Bioturbation substantially limits records of abrupt changes in sediments with accumulation rates below ~15 cm/kyr (e.g., McGee et al., 2013; Tierney et al., 2017). Records reflecting large regions, such as river runoff records from the Nile and Niger watersheds or pollen and leaf wax data from sites receiving long-traveled inputs, are likely to smooth variability. Finally, groundwater inputs to many lake and wetland sites, such as Lake Yoa, may cause a lagged response to precipitation changes (Eggermont et al., 2008; Grenier et al., 2009; Lézine et al., 2011).

These factors may explain the gradual drying observed in some records, but high-resolution records from Lake Bosumtwi (Shanahan et al., 2015) and from the Niger River mouth (Weldeab et al., 2007B) clearly indicate that the end of the AHP was more gradual at low latitudes than near the monsoon edges. Even in the Sahara and Sahel, several modeling studies find that vegetation-climate and dust-climate feedbacks are spatially variable (Brovkin & Claussen, 2008; Pausata et al., 2016; Renssen, Brovkin, Fichifet, & Goose, 2003; Williams et al., 2016), highlighting the fact that these feedbacks are not expected to lead to step-like drying in all regions.

Compilations of paleodata from North Africa suggest that the end of the AHP was time-transgressive over several millennia, with drying beginning earlier in the east and north and proceeding to the south and west (Figure 6C) (Kuper & Kröpelin, 2006; Shanahan et al., 2015; Tierney et al., 2017). This finding is consistent with orbital monsoonal theory, which suggests that the intensity of the African monsoonal rainfall and its northward penetration tracks orbital insolation forcing that establishes the land-sea summer monsoonal pressure gradient (Kutzbach & Guetter, 1986). It is difficult, however, to assess the abruptness of the end of the AHP in specific regions using compilations, given their inherent tendency to smooth temporal variability due to dating uncertainties,

bioturbation, and the inclusion of datasets with varying temporal resolutions. Despite these smoothing tendencies, some compilations suggest a more rapid drying at 6–5 ka superimposed on a more gradual mid-Holocene decline in monsoon strength, such as the reconstruction in the area covered by dated lake and wetland deposits of Lézine et al. (2011) and a compilation of radiocarbon dates from archaeological sites from all of North Africa (Figure 6B) (Manning & Timpson, 2014).

Conclusions

Proxy records provide extensive evidence for a wet period in the early Holocene that impacted essentially all of North Africa. Pollen data suggest that Sahelian steppe and savanna vegetation expanded throughout most of the northern Sahara (Bartlein et al., 2011; Jolly et al., 1998; Watrin et al., 2009); large lakes developed as far north as the Fazzan basin (26˚N) (Drake et al., 2008); dust deposition dropped by a factor of 2–5 even at sites near the northern edge of the Sahara (McGee et al., 2013); records of the isotopic composition of precipitation document summer monsoon rainfall as far north as 31˚N (Tierney et al., 2017); and human settlements extended across the Sahara (Manning & Timpson, 2014).

Many records indicate a rapid onset of the AHP at ~14.5 ka, in conjunction with the beginning of the BA warm period in the Northern Hemisphere, and most records with sufficient resolution document a decline in precipitation and increase in northeasterly winds during the YD cold period. Lake, pollen, river runoff, and leaf wax δD records consistently indicate that the peak of the AHP was achieved at ~10–8 ka, slightly after the peak insolation at 10–11 ka. Dust records contrast with these hydrological records, as minimum dust fluxes are achieved at 8–6 ka (Adkins et al., 2006; Cockerton et al., 2014; McGee et al., 2013; Williams et al., 2016). River runoff records document reductions in monsoon strength during Holocene cooling events such as the 8.2 ka event (Rohling et al., 2015; Weldeab et al., 2007B; Weldeab et al., 2014), but other proxy records do not generally have the resolution to document these centennial-scale events.

Following the peak of the AHP at ~10–8 ka, monsoon strength and extent decline, with locations at the eastern and northern edges of the West African monsoon showing the earliest impacts of this weakening. A dry interval occurs at ~8–7 ka in several sites (Tierney et al., 2017), though further work is necessary to demonstrate that this event is synchronous. At ~5 ka, several sites north and east of the modern summer monsoon extent show evidence for a locally rapid end of the AHP. Sites closer to the monsoon core (e.g., south of ~15˚N in West Africa) and reflecting larger spatial scales (e.g., runoff records from large river catchments) record a more gradual AHP termination, with the end of the AHP occurring as late as 3 ka at sites closer to the equator.

Several key areas remain for future work to better understand the response of North African climate to insolation forcing during the AHP. First, the importance of vegetation, lakes and dust as amplifiers of AHP climate remains unclear. Improved records of the time history of vegetation and lake area changes across North Africa will greatly assist efforts to test cause and effect. Model intercomparison studies and transient simulations involving these feedbacks will also be essential to increasing confidence in estimates of their importance. These simulations will also assist in identifying the importance of human-influenced changes in vegetation, lake extent, and dust emissions in shaping North African climate today.

Second, the drivers of the lagged precipitation response to insolation forcing in the early Holocene remain unclear. As yet it is not known whether this lag primarily reflects the evolution of Northern Hemisphere high-latitude climate (the early Holocene melting of ice sheets and warming of high-latitude oceans) or the slow onset of land surface feedbacks as vegetation migrated northward (Watrin et al., 2009) and aquifers filled, allowing lakes and wetlands to be established (Lézine et al., 2011). Improved records from previous humid periods may assist in understanding these lags, as other humid periods will have different time histories of high-latitude climate changes but should have generally similar lags related to local land surface responses.

Third, the variability of monsoon strength during the AHP remains poorly characterized and understood. While some records show simple, seemingly linear responses to high-latitude cooling events during the Holocene (e.g., river runoff records), others show evidence for centennial- to-millennial-scale dry periods (e.g., Lake Chad lake level, Lake Bostumwi Lake level and δD_{wax}) or rapid changes in atmospheric circulation (e.g., the δD_{wax} record from Lake Tana) between 9–6 ka that do not have a clear relationship to high-latitude forcings. These indications of prolonged mid-AHP drying may reflect local changes in the seasonal range of monsoon rains (Costa et al., 2014; Shanahan et al., 2015). Alternatively, mid-Holocene drying may be triggered by high-latitude cooling at 8.2 ka and extended to millennial timescales by vegetation and lake area feedbacks (Tierney et al., 2017).

Future research can also aim to develop a more comprehensive, mechanistic understanding of the impacts of end-AHP climate change on human societies. The temporal correspondence between the drying of the Sahara and the abandonment of human settlements is well established, but it is less clear how ecology, lifestyles, diets, and genomic diversity were impacted as monsoon strength waned. Were these human migrations orderly and structured or were they associated with duress and adaptation? Detailed study of archaeological remains, tooth and bone chemistry, pollen, and genomics may provide exciting new insights into the response of Saharan societies to mid-Holocene climate change.

Finally, the question of abrupt vs. gradual change at the end of the AHP remains unanswered. Progress in understanding the existence and extent of rapid drops in monsoon strength during the end of the AHP will rely on development of new high-

resolution records, improvements in our understanding of the climatic information contained in existing records showing abrupt responses at ~5 ka, and additional efforts to test whether records showing gradual changes reflect smoothing processes (e.g., low resolution sampling, imprecise dating, bioturbation, or systems with long response times) or a truly gradual decline in monsoon strength.

Efforts aimed at solving these and other remaining mysteries of the AHP will increase the utility of this remarkable, well-documented period for studies of the dynamics of precipitation responses to climate changes (Bony et al., 2015). Further research will also assist in improving our understanding of the ways that African humid periods impacted ecosystem development, human migration and human societies.

Suggested Reading

Drake, N. A., Blench, R. M., Armitage, S. J., Bristow, C. S., & White, K. H. (2011). **Ancient watercourses and biogeography of the Sahara explain the peopling of the desert**. *Proceedings of the National Academy of Sciences*, *108*(2), 458–462.

Kuper, R., & Kröpelin, S. (2006). **Climate-controlled Holocene occupation in the Sahara: Motor of Africa's evolution**. *Science*, *313*(5788), 803–807.

Manning, K., & Timpson, A. (2014). **The demographic response to Holocene climate change in the Sahara**. *Quaternary Science Reviews*, *101*, 28–35.

McGee, D., deMenocal, P. B., Winckler, G., Stuut, J. B. W., & Bradtmiller, L. I. (2013). **The magnitude, timing and abruptness of changes in North African dust deposition over the last 20,000 yr**. *Earth and Planetary Science Letters, 371–372*, 163–176.

deMenocal, P. B., & Tierney, J. E. (2012). African Humid Periods paced by Earth's orbital changes. *Nature Education*, *3*, 12.

Shanahan, T. M., McKay, N. P., Hughen, K. A., Overpeck, J. T., Otto-Bliesner, B., Heil, C. W., … Peck, J. (2015). **The time-transgressive termination of the African Humid Period**. *Nature Geoscience*, *8*(January), 140–144.

Tierney, J. E., & deMenocal, P. B. (2013). **Abrupt shifts in Horn of Africa hydroclimate since the last glacial maximum**. *Science*, *342*(6160), 843–846.

References

Adkins, J., deMenocal, P., & Eshel, G. (2006). **The "African Humid Period" and the record of marine upwelling from excess 230Th in ocean drilling program hole 658C**. *Paleoceanography*, *21*(4), 1–14.

Agency, I. A. E. (2007). *Report RAF/8/036*. Vienna.

Albani, S., Mahowald, N. M., Perry, A. T., Scanza, R. A., Zender, C. S., Heavens, N. G., … Otto-Bliesner, B. L. (2014). **Improved dust representation in the community atmosphere model**. *Journal of Advances in Modeling Earth Systems*, *6*, 541–570.

Albani, S., Mahowald, N. M., Winckler, G., Anderson, R. F., Bradtmiller, L. I., Delmonte, B., … Sun, J. (2015). **Twelve thousand years of dust: The Holocene global dust cycle constrained by natural archives**. *Climate of the Past*, *11*(6), 869–903.

Alley, R. B., Mayewski, P. A., Sowers, T., Stuiver, M., Taylor, K. C., & Clark, P. U. (1997). Holocene climatic instability: A prominent, widespread event 8,200 years ago. *Geology*, *25*, 483–486.

Andersen, K. K., Azuma, N., Barnola, J.-M., Bigler, M., Biscaye, P., Caillon, N., … White, J. W. C. (2004). **High-resolution record of Northern Hemisphere climate extending into the last interglacial period**. *Nature*, *431*(September), 147–151.

Armitage, S. J., Bristow, C. S., & Drake, N. A. (2015). **West African monsoon dynamics inferred from abrupt fluctuations of Lake Mega-Chad**. *Proceedings of the National Academy of Sciences*, *112*(28), 8543–8548.

Armitage, S. J., Drake, N. A., Stokes, S., El-Hawat, A., Salem, M. J., White, K., … McLaren, S. J. (2007). **Multiple phases of North African humidity recorded in lacustrine sediments from the Fazzan basin, Libyan Sahara**. *Quaternary Geochronology*, *2*(1–4), 181–186.

Bard, E., Rostek, F., Turon, J.-L., & Gendreau, S. (2000). **Hydrological impact of Heinrich events in the subtropical Northeast Atlantic**. *Science*, *289*(5483), 1321–1324.

Barth, H. (1857). *Travels and discoveries in North and Central Africa*. New York: Harper.

Bartlein, P. J., Harrison, S. P., Brewer, S., Connor, S., Davis, B. A. S., Gajewski, K., … Wu, H. (2011). **Pollen-based continental climate reconstructions at 6 and 21 ka: A global synthesis**. *Climate Dynamics*, *37*(3–4), 775–802.

Berger, A., & Loutre, M. F. (1991). **Insolation values for the climate of the last 1,000,000 years**. *Quaternary Science Reviews*, *10*(4), 297–317.

Bony, S., Stevens, B., Frierson, D. M. W., Jakob, C., Kageyama, M., Pincus, R., … Webb, M. J. (2015). **Clouds, circulation and climate sensitivity**. *Nature Geoscience*, *8*(4), 261–268.

Box, M. R., Krom, M. D., Cliff, R. A., Bar-Matthews, M., Almogi-Labin, A., Ayalon, A., & Paterne, M. (2011). **Response of the Nile and its catchment to millennial-scale climatic change since the LGM from Sr isotopes and major elements of East Mediterranean sediments**. *Quaternary Science Reviews*, *30*(3–4), 431–442.

Braconnot, P., Harrison, S. P., Kageyama, M., Bartlein, P. J., Masson-Delmotte, V., Abe-Ouchi, A., … Zhao, Y. (2012). **Evaluation of climate models using palaeoclimatic data**. *Nature Climate Change*, *2*(6), 417–424.

Braconnot, P., Otto-Bliesner, B., Harrison, S., Joussaume, S., Peterchmitt, J. Y., Abe-Ouchi, A., … Zhao, Y. (2007). **Results of PMIP2 coupled simulations of the mid-Holocene and Last Glacial Maximum—Part 1: Experiments and large-scale features**. *Climate of the Past*, *3*(2), 261–277.

Bradtmiller, L. I., McGee, D., Awalt, M., Evers, J., Yerxa, H., Kinsley, C. W., & DeMenocal, P. B. (2016). **Changes in biological productivity along the Northwest African margin over the past 20,000 years**. *Paleoceanography*, *31*, 1–18.

Brovkin, V., & Claussen, M. (2008). **Comment on "Climate-Driven Ecosystem Succession in the Sahara : The Past 6000 Years"**. *Science*, *322*(5906), 1326b.

Casford, J. S. L., Rohling, E. J., Abu-Reid, R., Cooke, S., Fontanier, C., Leng, M., & Lykousis, V. (2002). **Circulation changes and nutrient concentrations in the late Quaternary Aegean Sea: A nonsteady state concept for sapropel formation**. *Paleoceanography*, *17*(2), PA4215.

Castañeda, I. S., Mulitza, S., Schefuß, E., dos Santos, R. A. L., Damste, J. S. S., & Schouten, S. (2009). **Wet phases in the Sahara/Sahel region and human migration patterns in North Africa**. *Proceedings of the National Academy of Sciences of the United States of America*, *106*(48), 20159–20163.

Charney, J. G. (1975). Dynamics of deserts and drought in the Sahel. *Quarterly Journal of the Royal Meteorological Society*, *101*(1975), 193–202.

Claussen, M. (2009). Late Quaternary vegetation-climate feedbacks. *Climate of the Past*, *5*, 203–216.

Claussen, M., Brovkin, V., Ganopolski, A., Kubatzki, C., & Petoukhov, V. (1998). **Modelling global terrestrial vegetation climate interaction**. *Philosophical Transactions of the Royal Society of London Series B-Biological Sciences*, *353*(1365), 53–63.

Claussen, M., Dallmeyer, A., & Bader, J. (2017). Theory and Modeling of the African Humid Period and the Green Sahara. *Oxford Research Encyclopedia of Climate Science*. Retrieved from **http://climatescience.oxfordre.com/view/10.1093/acrefore/9780190228620.001.0001/acrefore-9780190228620-e-532**.

Claussen, M., Kubatzki, C., Brovkin, V., Ganopolski, A., Biogeochemie, M., & Joachim, H. (1999). **Simulation of an abrupt change in Saharan vegetation in the mid-Holocene**. *Geophysical Research Letters*, *26*(14), 2037–2040.

Cockerton, H. E., Holmes, J. A., Street-Perrott, F. A., & Ficken, K. J. (2014). **Holocene dust records from the West African Sahel and their implications for changes in climate and land surface conditions**. *Journal of Geophysical Research: Atmospheres*, *119*, 8684–8694.

Coe, M. T., & Bonan, G. B. (1997). **Feedbacks between climate and surface water in Northern Africa during the middle Holocene**. *Journal of Geophysical Research: Atmospheres*, *102*(D10), 11087–11101.

Coe, M. T., & Foley, J. A. (2001). **Human and natural impacts on the water resources of the Lake Chad basin**. *Journal of Geophysical Research*, *106*(2000), 3349.

Cole, J. M., Goldstein, S. L., deMenocal, P. B., Hemming, S. R., & Grousset, F. E. (2009). **Contrasting compositions of Saharan dust in the eastern Atlantic Ocean during the last deglaciation and African Humid Period**. *Earth and Planetary Science Letters*, *278*(3–4), 257–266.

Collins, J. A., Govin, A., Mulitza, S., Heslop, D., Zabel, M., Hartmann, J., … Wefer, G. (2013). **Abrupt shifts of the Sahara-Sahel boundary during Heinrich stadials**. *Climate of the Past*, *9*(3), 1181–1191.

Collins, J. A., Schefuß, E., Heslop, D., Mulitza, S., Prange, M., Zabel, M., … Wefer, G. (2011). **Interhemispheric symmetry of the tropical African rainbelt over the past 23,000 years**. *Nature Geoscience*, *4*(1), 42–45.

Collins, J. A., Schefuß, E., Mulitza, S., Prange, M., Werner, M., Tharammal, T., … Wefer, G. (2013). **Estimating the hydrogen isotopic composition of past precipitation using leaf-waxes from Western Africa**. *Quaternary Science Reviews*, *65*, 88–101.

Contoux, C., Jost, A., Ramstein, G., Sepulchre, P., Krinner, G., & Schuster, M. (2013). **Megalake Chad impact on climate and vegetation during the late Pliocene and the mid-Holocene**. *Climate of the Past*, *9*(4), 1417–1430.

Costa, K., Russell, J., Konecky, B., & Lamb, H. (2014). **Isotopic reconstruction of the African Humid Period and Congo Air Boundary migration at Lake Tana, Ethiopia**. *Quaternary Science Reviews*, *83*, 58–67.

Cremaschi, M. (2002). Late Pleistocene and Holocene climatic changes in the central Sahara. The case study of the Southwestern Fezzan, Libya. In F. A. Hassan (Ed.), *Droughts, food and culture: Ecological change and food security in Africa's later prehistory* (pp. 65–81). Boston: Springer.

Dansgaard, W. (1964). **Stable isotopes in precipitation**. *Tellus*, *16*(4), 436–468.

De Lange, G. J., Thomson, J., Reitz, A., Slomp, C. P., Principato, M. S., Erba, E., & Corselli, C. (2008). **Synchronous basin-wide formation and redox-controlled preservation of a Mediterranean sapropel**. *Nature Geoscience*, *1*(9), 606–610.

deMenocal, P. B. (1995). Plio-Pleistocene African climate. *Science*, *270*, 53–59.

deMenocal, P. B. (2008). **Palaeoclimate: Africa on the edge**. *Nature Geoscience*, *1*(October), 650–651.

deMenocal, P. B. (2015). **End of the African Humid Period**. *Nature Geoscience*, *8*(2), 86–87.

deMenocal, P., Ortiz, J., Guilderson, T., Adkins, J., Sarnthein, M., Baker, L., & Yarusinsky, M. (2000). **Abrupt onset and termination of the African Humid Period: Rapid climate responses to gradual insolation forcing**. *Quaternary Science Reviews*, *19*(1–5), 347–361.

Doherty, O. M., & Evan, A. T. (2014). **Identification of a new dust-stratocumulus indirect effect over the tropical North Atlantic**. *Geophysical Research Letters*, *41*(1), 6935–6942.

Drake, N. A., Blench, R. M., Armitage, S. J., Bristow, C. S., & White, K. H. (2011). **Ancient watercourses and biogeography of the Sahara explain the peopling of the desert**. *Proceedings of the National Academy of Sciences*, *108*(2), 458–462.

Drake, N. A., El-Hawat, A. S., Turner, P., Armitage, S. J., Salem, M. J., White, K. H., & McLaren, S. (2008). **Palaeohydrology of the Fazzan basin and surrounding regions: The last 7 million years**. *Palaeogeography, Palaeoclimatology, Palaeoecology*, *263*(3–4), 131–145.

Drake, N., & Bristow, C. (2006). **Shorelines in the Sahara: Geomorphological evidence for an enhanced monsoon from palaeolake Megachad**. *Holocene*, *16*(6), 901–911.

Dupont, L. (2011). **Orbital scale vegetation change in Africa**. *Quaternary Science Reviews*, *30*(25–26), 3589–3602.

Dupont, L. M., Beug, H. J., Stalling, H., & Tiedemann, R. (1989). 6. First palynological results from site 658 at 21 N off. *Northwest Africa: Pollen as Climate Indicators*, *108*, 93–111.

Dyke, A. S. (2004). **An outline of North American deglaciation with emphasis on Central and Northern Canada**. *Developments in Quaternary Science*, *2*(Part B), 373–424.

Egerer, S., Claussen, M., Reick, C., & Stanelle, T. (2015). **Marine sediment records as indicator for the changes in Holocene Saharan landscape: Simulating the dust cycle**. *Climate of the Past Discussions*, *11*(6), 5269–5306.

Egerer, S., Claussen, M., Reick, C., & Stanelle, T. (2016). **The link between marine sediment records and changes in Holocene Saharan landscape: Simulating the dust cycle**. *Climate of the Past*, *12*(4), 1009–1027.

Egerer, S., Claussen, M., Reick, C., & Stanelle, T. (2017). **Could gradual changes in Holocene Saharan landscape have caused the observed abrupt shift in North Atlantic dust deposition**? *Earth and Planetary Science Letters*, *473*, 104–112.

Eggermont, H., Verschuren, D., Fagot, M., Rumes, B., Van Bocxlaer, B., & Kröpelin, S. (2008). **Aquatic community response in a groundwater-fed desert lake to Holocene desiccation of the Sahara**. *Quaternary Science Reviews*, *27*(25–26), 2411–2425.

Ehrmann, W., Seidel, M., & Schmiedl, G. (2013). **Dynamics of late quaternary North African humid periods documented in the clay mineral record of central Aegean Sea sediments**. *Global and Planetary Change*, *107*, 186–195.

Evan, A. T., Vimont, D. J., Heidinger, A. K., Kossin, J. P., & Bennartz, R. (2009). **The role of aerosols in the evolution of tropical North Atlantic Ocean temperature anomalies**. *Science*, *324*(5928), 778–781.

Faure, H., Manguin, E., & Nydal, R. (1963). Formations lacustres du Quaternaire au Niger oriental. Diatomées et âges absolus. *Bulletin Du Bureau de Recherches Géologiques et Minières*, *3*, 41–63.

Fraedrich, K. (2015). **A minimalist model of terminal lakes: Qinghai Lake (China) and Lake Chad (N Africa)**. *Hydrology Research*, *46*(2), 222–231.

Francus, P., von Suchodoletz, H., Dietze, M., Donner, R. V., Bouchard, F., Roy, A. J., … Kröpelin, S. (2013). **Varved sediments of Lake Yoa (Ounianga Kebir, Chad) reveal progressive drying of the Sahara during the last 6100 years**. *Sedimentology*, *60*(4), 911–934.

Ganopolski, A., Kubatzki, C., Claussen, M., Brovkin, V., & Petoukhov, V. (1998). **The influence of vegetation-atmosphere-ocean interaction on climate during the mid-Holocene**. *Science*, *280*(5371), 1916–1919.

Garcin, Y., Melnick, D., Strecker, M. R., Olago, D., & Tiercelin, J. J. (2012). **East African mid-Holocene wet-dry transition recorded in palaeo-shorelines of Lake Turkana, northern Kenya Rift**. *Earth and Planetary Science Letters*, *331–332*, 322–334.

Gasse, F. (2000). **Hydrological changes in the African tropics since the Last Glacial Maximum**. *Quaternary Science Reviews*, *19*, 189–211.

Gasse, F., & Van Campo, E. (1994). **Abrupt post-glacial climate events in West Asia and North Africa monsoon domains**. *Earth and Planetary Science Letters*, *126*(4), 435–456.

Ghoneim, E., Benedetti, M., & El-Baz, F. (2012). **An integrated remote sensing and GIS analysis of the Kufrah Paleoriver, eastern Sahara**. *Geomorphology*, *139–140*, 242–257.

Gillespie, R., Street-Perrott, F. A., & Switsur, R. (1983). **Post-glacial arid episodes in Ethiopia have implications for climate prediction**. *Nature*, *306*(5944), 680–683.

Grenier, C., Paillou, P., & Maugis, P. (2009). **Assessment of Holocene surface hydrological connections for the Ounianga Lake catchment zone (Chad)**. *Comptes Rendus—Geoscience*, *341*(8–9), 770–782.

Gu, Y., Liou, K. N., Jiang, J. H., Su, H., & Liu, X. (2012). **Dust aerosol impact on North Africa climate: A GCM investigation of aerosol-cloud-radiation interactions using A-train satellite data**. *Atmospheric Chemistry and Physics*, *12*(4), 1667–1679.

Gumnior, M., & Preusser, F. (2007). Late Quaternary river development in the southwest Chad Basin: OSL dating of sediment from the Komadugu palaeofloodplain (northeast Nigeria). *Journal of Quaternary Science*, *22*(7), 709–719.

Harris, I., Jones, P. D., Osborn, T. J., & Lister, D. H. (2014). **Updated high-resolution grids of monthly climatic observations—the CRU TS3.10 dataset**. *International Journal of Climatology*, *34*, 623–642.

Hély, C., Lézine, A.-M., & Contributors, A. (2014). **Holocene changes in African vegetation: Tradeoff between climate and water availability**. *Climate of the Past*, *10*(2), 681–686.

Hoelzmann, P., Gasse, F., Dupont, L., Salzmann, U., Staubwasser, M., Leuschner, D. C., & Sirocko, F. (2004). Palaeoenvironmental changes in the arid and subarid belt (Sahara-Sahel-Arabian Peninsula) from 150 kyr to present. In R. W. Batterbee & E. Al (Eds.), *Past climate variability through Europe and Africa* (pp. 219–256). Dordrecht, The Netherlands: Springer.

Hoelzmann, P., Jolly, D., Harrison, S. P., Laarif, F., Bonnefille, R., & Pachur, H.-J. (1998). Mid-Holocene land-surface conditions in Northern Africa and the Arabian Peninsula: A data set for the analysis of biogeophysical feedbacks in the climate system. *Global Biogeochemical Cycles*, *12*(1), 35–51.

Hoelzmann, P., Kruse, H. J., & Rottinger, F. (2000). **Precipitation estimates for the eastern Saharan palaeomonsoon based on a water balance model of the West Nubian Palaeolake basin**. *Global and Planetary Change*, *26*(1–3), 105–120.

Huang, J., Zhang, C., & Prospero, J. M. (2009). **African aerosol and large-scale precipitation variability over West Africa**. *Environmental Research Letters*, *4*(1), 15006.

Jolly, D., Prentice, I. C., Bonnefille, R., Ballouche, A., Bengo, M., Brenac, P., … Waller, M. (1998). **Biome reconstruction from pollen and plant macrofossil data for Africa and the Arabian Peninsula at 0 and 6000 years**. *Journal of Biogeography*, *25*(6), 1007–1027.

Joussaume, S., Taylor, K. E., Braconnot, P., Mitchell, J. F. B., Kutzbach, J. E., Harrison, S. P., … Wyputta, U. (1999). **Monsoon changes for 6000 years ago: Results of 18 simulations from the Paleoclimate Modeling Intercomparison Project (PMIP)**. *Geophysical Research Letters*, *26*(7), 859–862.

Jung, S. J. A., Davies, G. R., Ganssen, G. M., & Kroon, D. (2004). **Stepwise Holocene aridification in NE Africa deduced from dust-borne radiogenic isotope records**. *Earth and Planetary Science Letters*, *221*(1–4), 27–37.

Kaufman, Y. J., Koren, I., Remer, L. A., Rosenfeld, D., & Rudich, Y. (2005). **The effect of smoke, dust, and pollution aerosol on shallow cloud development over the Atlantic Ocean**. *Proceedings of the National Academy of Sciences of the United States of America*, *102*(32), 11207–11212.

Krinner, G., Lézine, A. M., Braconnot, P., Sepulchre, P., Ramstein, G., Grenier, C., & Gouttevin, I. (2012). **A reassessment of lake and wetland feedbacks on the North African Holocene climate**. *Geophysical Research Letters*, *39*(7), 1–6.

Kröpelin, S., Verschuren, D., Lézine, A.-M., Eggermont, H., Cocquyt, C., Francus, P., … Engstrom, D. R. (2008). **Climate-driven ecosystem succession in the Sahara: The past 6000 years**. *Science*, *320*(5877), 765–768.

Kuechler, R. R., Schefuß, E., Beckmann, B., Dupont, L., & Wefer, G. (2013). **NW African hydrology and vegetation during the last glacial cycle reflected in plant-wax-specific hydrogen and carbon isotopes**. *Quaternary Science Reviews*, *82*, 56–67.

Kuper, R., & Kröpelin, S. (2006). **Climate-controlled Holocene occupation in the Sahara: Motor of Africa's evolution**. *Science*, *313*(5788), 803–807.

Kutzbach, J. E. (1980). **Estimates of past climate at Paleolake Chad, North Africa, based on a hydrological and energy-balance model**. *Quaternary Research*, *14*(2), 210–223.

Kutzbach, J. E. (1981). Monsoon climate of the early Holocene: climate experiment with the Earth's orbital parameters for 9000 years ago. *Science*, *214*, 59–61.

Kutzbach, J. E., & Guetter, P. J. (1986). **The influence of changing orbital parameters and surface boundary conditions on climate simulations of the past 18,000 years**. *Journal of the Atmospheric Sciences*, *43*(16), 1726–1759.

Lancaster, N., Kocurek, G., Singhvi, A., Pandey, V., Deynoux, M., Ghienne, J. F., & Lô, K. (2002). **Late Pleistocene and Halocene dune activity and wind regimes in the western Sahara Desert of Mauritania**. *Geology*, *30*(11), 991–994.

Larrasoaña, J. C., Roberts, A. P., Rohling, E. J., Winklhofer, M., & Wehausen, R. (2003). **Three million years of monsoon variability over the northern Sahara**. *Climate Dynamics*, *21*(7–8), 689–698.

Laskar, J., Fienga, A., Gastineau, M., & Manche, H. (2011). **La2010: A new orbital solution for the long term motion of the Earth**. *Astronomy & Astrophysics*, *532*, A89.

Lézine, A. M., Hély, C., Grenier, C., Braconnot, P., & Krinner, G. (2011). **Sahara and Sahel vulnerability to climate changes, lessons from Holocene hydrological data**. *Quaternary Science Reviews*, *30*(21–22), 3001–3012.

Lézine, A. M., Watrin, J., Vincens, A., & Hély, C. (2009). **Are modern pollen data representative of West African vegetation**? *Review of Palaeobotany and Palynology*, *156*(3–4), 265–276.

Lézine, A. M., & Casanova, J. (1989). Pollen and hydrological evidence for the interpretation of past climates in tropical west Africa during the Holocene. *Quaternary Science Reviews*, *8*(1), 45–55.

Manning, K., & Timpson, A. (2014). **The demographic response to Holocene climate change in the Sahara**. *Quaternary Science Reviews*, *101*, 28–35.

Marcella, M. P., & Eltahir, E. A. B. (2014). **The role of mineral aerosols in shaping the regional climate of West Africa**. *Journal of Geophysical Research: Atmospheres*, *119*(10), 5806–5822.

Marino, G., Rohling, E. J., Sangiorgi, F., Hayes, A., Casford, J. L., Lotter, A. F., … Brinkhuis, H. (2009). **Early and middle Holocene in the Aegean Sea: Interplay between high and low latitude climate variability**. *Quaternary Science Reviews*, *28*(27–28), 3246–3262.

Marshall, M. H., Lamb, H. F., Huws, D., Davies, S. J., Bates, R., Bloemendal, J., … Bryant, C. (2011). **Late Pleistocene and Holocene drought events at Lake Tana, the source of the Blue Nile**. *Global and Planetary Change*, *78*(3–4), 147–161.

McGee, D., deMenocal, P. B., Winckler, G., Stuut, J. B. W., & Bradtmiller, L. I. (2013). **The magnitude, timing and abruptness of changes in North African dust deposition over the last 20,000 yr**. *Earth and Planetary Science Letters*, *371–372*, 163–176.

Mercone, D., Thomson, J., Croudace, I. W., Siani, G., Paterne, M., & Troelstra, S. (2000). **Duration of S1, the most recent sapropel in the Eastern Mediterranean Sea, as**

indicated by accelerator mass spectrometry radiocarbon and geochemical evidence. *Paleoceanography*, *15*(3), 336–347.

Miller, R. L., Tegen, I., & Perlwitz, J. (2004). **Surface radiative forcing by soil dust aerosols and the hydrologic cycle**. *Journal of Geophysical Research: Atmospheres*, *109*(D4), D04023.

Möbius, J., Lahajnar, N., & Emeis, K.-C. (2010). **Diagenetic control of nitrogen isotope ratios in Holocene sapropels and recent sediments from the Eastern Mediterranean Sea**. *Biogeosciences*, *7*(11), 3901–3914.

Niedermeyer, E. M., Schefuss, E., Sessions, A. L., Mulitza, S., Mollenhauer, G., Schulz, M., & Wefer, G. (2010). **Orbital- and millennial-scale changes in the hydrologic cycle and vegetation in the western African Sahel: insights from individual plant wax delta D and delta C-13**. *Quaternary Science Reviews*, *29*(23–24), 2996–3005.

Pachur, H. J., & Kröpelin, S. (1987). **Wadi Howar: Paleoclimatic evidence from an extinct river system in the southeastern Sahara**. *Science*, *237*(4812), 298–300.

Paillou, P., Schuster, M., Tooth, S., Farr, T., Rosenqvist, A., Lopez, S., & Malezieux, J. M. (2009). **Mapping of a major paleodrainage system in Eastern Libya using orbital imaging radar: The Kufrah River**. *Earth and Planetary Science Letters*, *277*(3–4), 327–333.

Paillou, P., Tooth, S., & Lopez, S. (2012). **The Kufrah paleodrainage system in Libya: A past connection to the Mediterranean Sea**? *Comptes Rendus—Geoscience*, *344*(8), 406–414.

Patricola, C. M., & Cook, K. H. (2007). Dynamics of the West African monsoon under mid-Holocene precessional forcing: Regional climate model simulations. *Journal of Climate*, *20*(4), 694–716.

Patricola, C. M., & Cook, K. H. (2008). **Atmosphere/vegetation feedbacks: A mechanism for abrupt climate change over northern Africa**. *Journal of Geophysical Research*, *113*(September), 1–18.

Pausata, F. S. R., Messori, G., & Zhang, Q. (2016). **Impacts of dust reduction on the northward expansion of the African monsoon during the Green Sahara period**. *Earth and Planetary Science Letters*, *434*, 298–307.

Perez-Sanz, A., Li, G., González-Sampériz, P., & Harrison, S. P. (2014). **Evaluation of modern and mid-Holocene seasonal precipitation of the Mediterranean and Northern Africa in the CMIP5 simulations**. *Climate of the Past*, *10*(2), 551–568.

Pourmand, A., Marcantonio, F., & Schulz, H. (2004). **Variations in productivity and aeolian fluxes in the northeastern Arabian Sea during the past 110 ka**. *Earth and Planetary Science Letters*, *221*(1–4), 39–54.

Renssen, H., Brovkin, V., Fichefet, T., & Goosse, H. (2003). **Holocene climate instability during the termination of the African Humid Period**. *Geophysical Research Letters*, *30*(4), 1184.

Revel, M., Ducassou, E., Grousset, F. E., Bernasconi, S. M., Migeon, S., Revillon, S., … Bosch, D. (2010). **100,000 tears of African monsoon variability recorded in sediments of the Nile margin**. *Quaternary Science Reviews*, *29*(11–12), 1342–1362.

Ridley, D. A., Heald, C. L., & Prospero, J. M. (2014). **What controls the recent changes in African mineral dust aerosol across the Atlantic**? *Atmospheric Chemistry and Physics*, *14*(11), 5735–5747.

Risi, C., Bony, S., & Vimeux, F. (2008). **Influence of convective processes on the isotopic composition (delta O-18 and delta D) of precipitation and water vapor in the tropics: 2. Physical interpretation of the amount effect**. *Journal of Geophysical Research: Atmospheres*, *113*(D19).

Risi, C., Bony, S., Vimeux, F., Descroix, L., Ibrahim, B., Lebreton, E., … Sultan, B. (2008). **What controls the isotopic composition of the African monsoon precipitation? Insights from event-based precipitation collected during the 2006 AMMA field campaign**. *Geophysical Research Letters*, *35*(24), L24808.

Ritchie, J. C., & Haynes, C. V. (1987). **Holocene vegetation zonation in the eastern Sahara**. *Nature*, *330*(6149), 645–647.

Robinson, C. A., El-Baz, F., Al-Saud, T. S. M., & Jeon, S. B. (2006). **Use of radar data to delineate palaeodrainage leading to the Kufra Oasis in the eastern Sahara**. *Journal of African Earth Sciences*, *44*(2), 229–240.

Rohling, E. J., Marino, G., & Grant, K. M. (2015). **Mediterranean climate and oceanography, and the periodic development of anoxic events (sapropels)**. *Earth-Science Reviews*, *143*, 62–97.

Rosenfeld, D., Rudich, Y., & Lahav, R. (2001). **Desert dust suppressing precipitation: A possible desertification feedback loop**. *Proceedings of the National Academy of Sciences*, *98*(11), 5975–5980.

Rossignol-Strick, M. (1983). **African monsoons, an immediate climate response to orbital insolation**. *Nature*, *304*(5921), 46–49.

Le Roux, G., Fagel, N., De Vleeschouwer, F., Krachler, M., Debaille, V., Stille, P., … Shotyk, W. (2012). **Volcano- and climate-driven changes in atmospheric dust sources and fluxes since the late glacial in Central Europe**. *Geology*, *40*(4), 335–338.

Russell, J., Talbot, M. R., & Haskell, B. J. (2003). **Mid-Holocene climate change in Lake Bosumtwi, Ghana**. *Quaternary Research*, *60*(2), 133–141.

Sachs, J. P., & Repeta, D. J. (1999). **Oligotrophy and nitrogen fixation during eastern Mediterranean sapropel events**. *Science*, *286*(5449), 2485–2488.

Sachse, D., Billault, I., Bowen, G. J., Chikaraishi, Y., Dawson, T. E., Feakins, S. J., … Kahmen, A. (2012). **Molecular paleohydrology: Interpreting the hydrogen-isotopic composition of lipid biomarkers from photosynthesizing organisms**. *Annual Review of Earth and Planetary Sciences*, *40*(1), 221–249.

Sarnthein, M. (1978). **Sand deserts during glacial maximum and climatic optimum**. *Nature*, *272*, 43–46.

Shanahan, T. M., Hughen, K. A., McKay, N. P., Overpeck, J. T., Scholz, C. A., Gosling, W. D., … Heil, C. W. (2016). CO2 and fire influence tropical ecosystem stability in response to climate change. *Scientific Reports*, *6*(1), 517.

Shanahan, T. M., McKay, N. P., Hughen, K. A., Overpeck, J. T., Otto-Bliesner, B., Heil, C. W., … Peck, J. (2015). **The time-transgressive termination of the African Humid Period**. *Nature Geoscience*, *8*(January), 140–144.

Shanahan, T. M., Overpeck, J. T., Scholz, C. A., Beck, J. W., Peck, J., & King, J. W. (2008). **Abrupt changes in the water balance of tropical West Africa during the late Quaternary**. *Journal of Geophysical Research*, *113*(D1208), 1–12.

Shanahan, T. M., Overpeck, J. T., Wheeler, C. W., Beck, J. W., Pigati, J. S., Talbot, M. R., … King, J. W. (2006). **Paleoclimatic variations in West Africa from a record of late Pleistocene and Holocene lake level stands of Lake Bosumtwi, Ghana**. *Palaeogeography, Palaeoclimatology, Palaeoecology*, *242*(3–4), 287–302.

Skonieczny, C., Bory, A., Bout-Roumazeilles, V., Abouchami, W., Galer, S. J. G., Crosta, X., … Ndiaye, T. (2011). **The 7–13 March 2006 major Saharan outbreak: Multiproxy characterization of mineral dust deposited on the West African margin**. *Journal of Geophysical Research: Atmospheres*, *116*(18).

Skonieczny, C., Bory, A., Bout-Roumazeilles, V., Abouchami, W., Galer, S. J. G., Crosta, X., … Ndiaye, T. (2013). **A three-year time series of mineral dust deposits on the West African margin: Sedimentological and geochemical signatures and implications for interpretation of marine paleo-dust records**. *Earth and Planetary Science Letters*, *364*, 145–156.

Skonieczny, C., Paillou, P., Bory, A., Bayon, G., Biscara, L., Crosta, X., … Grousset, F. (2015). **African Humid Periods triggered the reactivation of a large river system in western Sahara**. *Nature Communications*, *6*, 8751.

Slowey, N. C., & Henderson, G. M. (2011). **Radiocarbon ages constraints on the origin and shedding of bank-top sediment in the Bahamas during the Holocene**. *Aquatic Geochemistry*, *17*(4), 419–429.

Street-Perrott, F. A., & Harrison, S. P. (1985). Lake levels and climate reconstruction. In Hecht, A. D. (Ed.), *Paleoclimate Analysis and Modeling* (pp. 291–340). New York: John Wiley.

Street-Perrott, F. A., Marchand, D. S., Roberts, N., & Harisson, S. (1989). *Global lake-level variations from 18,000 to 0 years ago: A paleoclimatic analysis*. U.S. Department of Energy Technical Report 46, Washington, DC.

Taylor, K. E., Stouffer, R. J., & Meehl, G. A. (2012). **An Overview of CMIP5 and the experiment design**. *Bulletin of the American Meteorological Society*, *93*, 485–498.

Tierney, J. E., & deMenocal, P. B. (2013). **Abrupt shifts in Horn of Africa hydroclimate since the Last Glacial Maximum**. *Science*, *342*(6160), 843–846.

Tierney, J. E., Lewis, S. C., Cook, B. I., LeGrande, A. N., & Schmidt, G. A. (2011). **Model, proxy and isotopic perspectives on the East African Humid Period**. *Earth and Planetary Science Letters*, *307*(1–2), 103–112.

Tierney, J. E., Pausata, F. S. R., & DeMenocal, P. B. (2017). **Rainfall regimes of the Green Sahara**. *Science Advances*, *3*(1), e1601503.

Tjallingii, R., Claussen, M., Stuut, J.-B. W., Fohlmeister, J., Jahn, A., Bickert, T., … Röhl, U. (2008). **Coherent high- and low-latitude control of the Northwest African hydrological balance**. *Nature Geoscience*, *1*(10), 670–675.

Trauth, M. H., Larrasoaña, J. C., & Mudelsee, M. (2009). **Trends, rhythms and events in Plio-Pleistocene African climate**. *Quaternary Science Reviews*, *28*(5–6), 399–411.

Tsoar, H. (2005). **Sand dunes mobility and stability in relation to climate**. *Physica A: Statistical Mechanics and Its Applications*, *357*(1), 50–56.

Ullman, D. J., LeGrande, A. N., Carlson, A. E., Anslow, F. S., & Licciardi, J. M. (2014). **Assessing the impact of Laurentide Ice Sheet topography on glacial climate**. *Climate of the Past*, *10*(2), 487–507.

Watrin, J., Lézine, A. M., Hély, C., Cour, P., Ballouche, A., Duzer, D., … Waller, M. P. (2009). **Plant migration and plant communities at the time of the “green Sahara”**. *Comptes Rendus—Geoscience*, *341*(8–9), 656–670.

Weldeab, S., Lea, D. W., Schneider, R. R., & Andersen, N. (2007a). **155,000 years of West African monsoon and ocean thermal evolution**. *Science*, *316*(5829), 1303–1307.

Weldeab, S., Lea, D. W., Schneider, R. R., & Andersen, N. (2007b). **Centennial scale climate instabilities in a wet early Holocene West African monsoon**. *Geophysical Research Letters*, *34*(24), 1–6.

Weldeab, S., Menke, V., & Schmiedl, G. (2014). **The pace of East African monsoon evolution during the Holocene**. *Geophysical Research Letters*, *41*, 1724–1731.

Williams, R. H., McGee, D., Ridley, D. A., Kinsley, C. W., Hu, S., Fedorov, A. V., … DeMenocal, P. B. (2016). Glacial to Holocene changes in trans-Atlantic Saharan dust transport and dust-climate feedbacks. *Science Advances*, *2*, e1600445.

Yoshioka, M., Mahowald, N. M., Conley, A. J., Collins, W. D., Fillmore, D. W., Zender, C. S., & Coleman, D. B. (2007). **Impact of desert dust radiative forcing on Sahel precipitation: Relative importance of dust compared to sea surface temperature variations, vegetation changes, and greenhouse gas warming**. *Journal of Climate*, *20*(8), 1445–1467.

Zhao, M., Beveridge, N. A. S., Shackleton, N. J., Sarnthein, M., & Eglinton, G. (1995). **Molecular stratigraphy of cores off Northwest Africa: Sea surface temperature history over the last 80 ka** *Paleoceanography*, *10*(3), 661–675.

Zhao, M., Dupont, L., Eglinton, G., & Teece, M. (2003). **N-alkane and pollen reconstruction of terrestrial climate and vegetation for N.W. Africa over the last 160 kyr**. *Organic Geochemistry*, *34*(1), 131–143.

David McGee

Earth, Atmospheric, and Planetary Sciences, Massachusetts Institute of Technology

Peter B. deMenocal

Department of Earth and Environmental Sciences, Columbia University; Lamont-Doherty Earth Observatory, Columbia University